# AN EXPERIMENTAL STUDY OF THE USE OF PLASMA ACTUATORS FOR SKIN FRICTION REDUCTION IN TURBULENT BOUNDARY LAYERS

A Thesis

by

CHRISTOPHER WADE RUSSO

Submitted to the Office of Graduate and Professional Studies of
Texas A&M University
in partial fulfillment of the requirements for the degree of

MASTER OF SCIENCE

| | |
|---|---|
| Chair of Committee, | Othon Rediniotis |
| Co-Chair of Committee, | Rodney Bowersox |
| Committee Members, | Diego Donzis |
| | Simon North |
| Head of Department, | Rodney Bowersox |

December 2016

Major Subject: Aerospace Engineering

## ABSTRACT

Parasitic drag is a restrictive force for all vehicles moving through a fluid medium. In many industries and applications, even incremental reductions in drag could result in large savings in fuel, time, and even thermal management. In turbulent flows, skin friction drag is of particular concern. The main source of turbulent skin friction drag is thought to be due to low-velocity streaks in the near-wall region of the boundary layer and by hairpin vortices which carry high-velocity flows further down into the boundary layer, resulting in higher local wall shear stress and higher drag. Computational work by Du and Karniadakis suggests that these two phenomena may be minimized using a force in the form of a span-wise traveling wave. Reductions in skin friction drag of over 50% were predicted. Several attempts have been made to reproduce this wave and the resultant reduction in drag in experiments. An actively-deformed skin design was examined by Rediniotis and Lagoudas, but this experiment's results were invalidated due to an irregularity in skin movement. Preliminary tests by Wilkinson, using oscillating surface plasma, failed to create an adequate effect and created a mean-flow region that complicated comparison to computational results. Still, this concept's large predicted reductions in drag provide an incentive for further investigation. This study deals with several wind tunnel tests undertaken in the fall of 2015 at the 3'x4' wind tunnel at Texas A&M University to evaluate a drag-reduction scheme designed by Lynntech, Inc. A NACA 0012 infinite wing with a $Re_c$ of 1.6 million was tested with embedded discrete plasma actuators in two different configurations. Hot film velocity measurements of the boundary layer were taken with and without the pulsed plasma

actuators engaged. Calculations of wall shear stress and friction coefficient indicated up to a 66% local reduction in drag. Baseline boundary layer measurements showed good agreement with existing computational and experimental data at similar Reynolds Numbers. Overall wing drag measurements using a pyramidal balance integral to the tunnel test section showed some signs of overall drag reduction, but were less conclusive than local measurements.

## DEDICATION

To my parents Louis and Phyllis Russo, my brother Michael, and my friends Beau Holder and Matt Sparks. Your love, patience, support, prayers, reassurance, and gracious tolerance of my choleric temperament have been invaluable throughout these years of work towards this thesis. I cannot thank you enough.

## ACKNOWLEDGMENTS

I would like to thank my advisor and committee co-chair, Dr. Rodney Bowersox, for giving me the opportunity to be a part of his research group, to work in his laboratory for several years, for many long meetings reasoning through complex fluid dynamics, and most of all for the patience and sincere belief in me that have allowed me to finish this endeavor I started. His guidance was instrumental in the completion of this thesis and in my growth as a person from the time I met him as a senior in pursuit of my Bachelor's Degree at Texas A&M in 2011.

Additionally, I would like to thank my committee chair, Dr. Othon Rediniotis, for giving me the opportunity to conduct this research, for his invaluable insight and support during data analysis and the process of preparing this document. I would like to thank the other members of my thesis committee, Dr. Diego Donzis and Dr. Simon North for their valuable knowledge and insight, expressed both in the insight given in the review of this thesis and in the classes of theirs that I have taken through my years of undergraduate and graduate education. Finally, I would like to thank Dr. Waruna Kulatilaka for assisting with the defense.

I would like to thank the members of the team from Lynntech who helped conduct this research, constructed the wing and plasma actuators, and performed a separate analysis of the data – Sibi Mathew, Wahaj Saleem, Ashwin Balasubramanian and Jesse Pedroni. Many thanks go to Ismael Vilchis, an undergraduate student worker whose proficiency with tools and incredible work ethic made this research possible on an extremely compressed testing schedule. Furthermore, I would like to thank Dr. Yogesh

Babbar for his help and insight into the hot film anemometry system and calibration of the pyramidal balance.

My sincerest gratitude goes out to all researchers at the National Aerothermochemistry Laboratory, past and present, for their invaluable support and insight whenever I needed it. In particular, my thanks go out to Dr. Chi Mai and Dr. Jerrod Hofferth, who taught me essentially everything I know about wind tunnel testing, data acquisition, preparing drawings for machining, purchasing, and much more. Also, thanks to Andrew Leidy and Ian Neel for their insight and advice over the years. I would like to thank all of the machinists, especially Will Seward, for great work in preparing parts for various experiments over my time both at the National Aerothermochemistry Laboratory and under Dr. Rediniotis.

Finally, I would like to thank Karen Knabe, Gail Rowe, Colleen Leatherman, and Rebecca Marianno, Aerospace Engineering staff members, for helping with my degree plan (including changes), scheduling, finances, paperwork, and meeting deadlines.

## TABLE OF CONTENTS

Page

Page

## LIST OF FIGURES

Page

Page

Page

## LIST OF TABLES

Page

# INTRODUCTION

## General

The investigation into active methods of reducing skin friction drag has been a subject of major interest within the aerodynamics community for many decades. The benefits of both active and passive skin friction reduction are obvious – with a rising demand for global connectivity and the transportation of goods and people around the globe, even marginal reductions of skin-friction drag can lead to massive cost savings in fuel costs and time. In high-speed applications, where thermal management is of utmost concern [1], reduction in turbulent drag could also save money in thermal shielding and material manufacturing.

It is useful to review several basic concepts in aerodynamics, including drag, boundary layers, and turbulence before moving forward. As any object moves through a fluid medium, it experiences aerodynamic forces due to both pressure and shear stress on the surface of the object. Drag is defined as the aerodynamic force acting on a body parallel with the relative velocity of the fluid flow over the body [2]. This drag may be broken down into the aforementioned components of pressure and shear stress. The drag due to shear stress is known as skin-friction drag. Because the total skin-friction drag is the integration of the shear stress distribution over the surface of an object, local drag due to skin friction may be considered to be equivalent to the shear stress at a specific point on the surface (often referred to as the wall). In Newtonian fluids, this shear stress may be related to the rate of change in the stream-wise velocity in the wall-normal direction at the wall [3]:

$$\tau_w = \mu \frac{\partial u}{\partial y}\Big|_{wall}$$

In order to compare the effect of this wall shear stress (sometimes shortened as "wall stress") on systems of differing scales, it is often helpful to introduce a non-dimensional friction coefficient, $C_f$, which may be expressed as follows[2]:

$$C_f = \frac{\tau_w}{\frac{1}{2}\rho {U_\infty}^2}$$

In this equation, $\rho$ is the density of the fluid and $U_\infty$ is the velocity in the freestream. This coefficient of friction provides a quantity that may offer a valid comparison of skin friction drag between different objects or locations, but it should be noted that various empirical studies have shown it to vary with local and global Reynolds Number [4]. The Reynolds Number (abbreviated Re) is a non-dimensional quantity expressed as follows:

$$Re = \frac{uL}{\nu}$$

In this equation, $u$ is the local velocity, $L$ represents some characteristic velocity (chord length, x-location, etc.), and $\nu$ is the fluid's kinematic viscosity. This quantity helps express the ratio of inertial to viscous forces in a given flow. It can also be a helpful indicator of whether a given flow is laminar or turbulent.

This brings up the important distinction between laminar and turbulent flow. In laminar flows, streamlines are very organized and smooth, with minimal disturbances quickly being canceled out. As a flow evolves over space and time in a process known as transition, these instabilities may grow until eventually they lead to seemingly disorderly

unsteady flows which we describe as turbulent [3]. This process over a flat plate is illustrated in Figure 1 below.

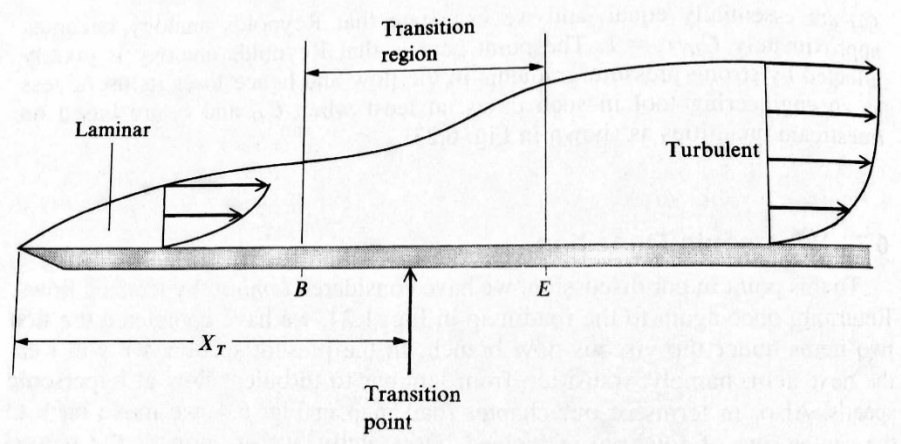


*Figure 1 - Transition from Laminar to Turbulent Flow Over a Flat Plate (Credit: Anderson)*

Turbulent boundary layers increase the skin friction drag on an object and this can be seen in their velocity profile – they have a fuller profile indicating a larger velocity gradient close to the wall and thus a higher wall shear stress, as discussed earlier in this section. Understanding and controlling turbulent boundary layers for reduction in skin friction is critical mainly because most real-world flows, such as the boundary layers on the wings of a commercial jet, behave turbulently [3].

**Wind Tunnel Testing**

One method of conducting aerodynamic experiments is to use a wind tunnel. Wind tunnels are machines designed to produce flows of air in a laboratory setting which simulate conditions of actual flight in the atmosphere [2], although some wind tunnels may be used to reach conditions necessary for the observation of specific fluid phenomena, even if these conditions are normally not found in flight. The use of these

devices goes back through the history of flight – the Wright brothers used a wind tunnel during the fall of 1901 to test several different airplane models for lift and drag over a range of angles of attack [5].

Two main types of wind tunnels exist – open-circuit tunnels where air is drawn in directly from the local atmosphere and closed-circuit tunnels (also called recirculating tunnels), which have redirect the exhaust of the tunnel back into the input to form a loop. The region of the wind tunnel with uniform velocity and usually some sort of instrumentation and optical access is referred to as the test section. This is where all experiments in a wind tunnel take place.

**Current Advances in Turbulent Skin Friction Reduction**

Turbulent boundary layers have several unique observed phenomena that are believed to contribute to skin-friction drag, including low-velocity streaks in the near-wall region [6] and elongated hairpin vortices starting in the near-wall region and extending through a large part of the boundary-layer and sometimes beyond it [7]. These structures are thought to be the primary source of turbulence production in the boundary layer.

Several approaches have sought to control turbulent production in order to reduce skin-friction drag by influencing the aforementioned features. Notably, riblets on the surface of a wall, inspired by the structures on shark skin, have been shown to reduce drag force by 5-10% [8].

Work by Du and Karniadakis used simulations of electromagnetic tiles (similar in concept to plasma actuators) in a salt water channel flow to propose that a much

greater reduction in skin friction in turbulent boundary layers may be achieved through the application of a span-wise traveling wave force applied in the near-wall region and decaying exponentially in the wall-normal direction [9]. This force takes the form

$$F_z = Ie^{-y/\Delta} \sin\left(\frac{2\pi}{\lambda_z} z - \frac{2\pi}{T} t\right)$$

where $I$ is the amplitude of the excitation, $\Delta$ is the penetration length of the force, $\lambda_z$ is the wavelength along the span, and $T$ is the period. This method weakened and sometimes eliminated near-wall velocity streaks, leaving instead a near-wall low velocity region. This resulted in a reduction in drag of more than 50% in some cases (although computational), making it an extremely promising approach for further experimentation.

Several different attempts have been made to take advantage of this principle in experiments. Rediniotis, Lagoudas, Mani, Traub, Allen, and Karniadakis performed a set of computational and experimental studies using a so-called "smart" skin which deformed the wall surface to take the shape of the traveling wave to eliminate near-wall streaks [10]. However, irregular motion of cams which controlled the skin deformation invalidated experimental results, which were not included in studies. In addition, Wilkinson attempted to use a surface plasma along surface strip electrodes in order to achieve a similar effect as the traveling wave [11]. This testing was stopped at the bench-top level before full-scale wind tunnel testing due to an inability to achieve a moving wave effect at low frequencies and a mean flow generated by the moving surface plasma. Later, experiments with oscillating flow plasma actuators by Jukes, Choi, Johnson, and Scott managed to achieve a maximum local reduction in skin friction

of 45% downstream of the actuators [12]. However, the method of action in the latter approach is fundamentally different from the approach described by Du and Karniadakis in that it is related to the action of the Stokes layer rather than stabilization of near-wall streaks [9].

**Research Summary and Goals**

The main purpose of this study was to investigate the possibility of a reduction in drag due to skin friction of a configuration designed by Lynntech, Inc. To date, the author of this thesis has found no experiments successfully implementing the span-wise traveling wave for turbulent skin-friction drag reduction. Although several attempts were made immediately following the publication of the findings of Du and Karniadakis, none of them were successful.

Given the potentially costly and hard-to-maintain nature of an actively-deforming surface and the complications of surface plasma strips, it is believed that discrete embedded actuators may prove a more practical way of implementing the span-wise traveling wave if they are proven to be effective in reducing skin-friction drag. During the fall of 2015, several experiments were conducted at Texas A&M University, using fixed discrete pulsed plasma actuators in several configurations on an infinite wing design. This project was funded through NASA SBIR contract #NNX15CL61P awarded to Lynntech with Texas A&M as a sub-contractor. Lynntech designed and fabricated this wing and plasma actuators. The operation and parameters associated with plasma actuator operation (e.g. voltage, pulse duration, frequency, and location) were also determined by Lynntech personnel. Lynntech personnel were present and assisted with

wind tunnel testing at Texas A&M University, with a test matrix determined by Lynntech. Skin friction drag was measured by taking boundary layer velocity measurements at several locations and calculating the wall shear stress $\tau_w$ and the friction coefficient $C_f$ at each location. Additionally, measurements of the total drag on the wing using a pyramidal balance installed on the model sting in the wind tunnel test section. The goal of these measurements was to demonstrate local reductions in skin-friction drag in turbulent boundary layers over the wing. After testing, an analysis of test data was independently conducted by Lynntech and data shared with Texas A&M in December 2015. Analysis reported in this thesis used insights from this analysis in the author's examination of the test data.

## EXPERIMENTAL CONFIGURATION AND METHODS

### Overview

Experimental testing took place at Texas A&M University in the 3'x4' low-speed wind tunnel at a target velocity of 40 m/s and a target $Re_c$ of 1.6 million. The primary objective of this testing was to take boundary-layer measurements at various points in both the stream-wise and span-wise directions along a wing both with and without pulsed plasma actuators.

In order to achieve very sensitive velocity and power spectrum measurements within the boundary layer, CTA was employed using a TSI IFA 300 Constant Temperature Anemometer System with a TSI Model 1201 hot film probe mounted using a TSI Model 1150 standard probe support. Data was acquired using a National Instruments USB-6211 Data Acquisition (DAQ) card and the MATLAB Data Acquisition Toolbox. Each of these components will be discussed in further detail in the proceeding subsections.

In order take precise velocity measurements close to the surface of the wing without creating interference, the TSI Model 1201 hot film probe and probe support were mounted on the vertical traversing sting at a 15-degree downward angle relative to the horizontal (stream-wise direction). The hot film was aligned so that it was oriented along the span-wise direction and was parallel to the wing surface. This was so that it would capture the stream-wise velocity. It was assumed that the velocity in the surface-normal direction in the boundary layer would be minimal due to the no-penetration condition. The plasma actuators in this experiment produce a jet with a velocity

component normal to the wall, but this contribution is thought to be minimal even a short distance away from the actuators themselves and care was taken to place the probe a sufficient distance away so that no wall-normal component was measured. Additionally, any additional wall-normal component would be read as an increase in total velocity near the wall, resulting in a higher wall shear stress and thus increased drag. Any reductions in drag measured, then, would be unaffected by this factor.

**Texas A&M 3'x4' Low-Speed Wind Tunnel**

The Texas A&M 3'x4' Low-Speed Wind Tunnel is located in the Aero and Fluid Dynamics Lab on the campus of Texas A&M University in College Station, Texas. It so-named for the 3'x4' rectangular test section. This recirculating wind tunnel operates at atmospheric stagnation pressure at velocities from 0 to ~45 m/s, controlled by adjusting the RPM of the driving propeller motor. A simple pitot prove is mounted just upstream of the test section in order to measure the freestream pressure and velocity.

One unique feature of this wind tunnel is that it can be used to perform multiple experiments without significant setup time. Three separate test sections with different traversing mechanisms, force balances, and other hardware may be rolled into place by two to four people with relative ease. Because this configuration does not provide a total seal, the tunnel operates at local atmospheric pressure.

This particular test section is equipped with a 3-dimensional traversing system which may be used to position a probe support at various points throughout the tunnel. This probe support was used as a mount for a CTA hot film probe. Additionally, the

model support sting in this tunnel is attached to a pyramidal balance that measures lift, drag, and pitching moment. This Pyramidal balance is shown in Figure 2.

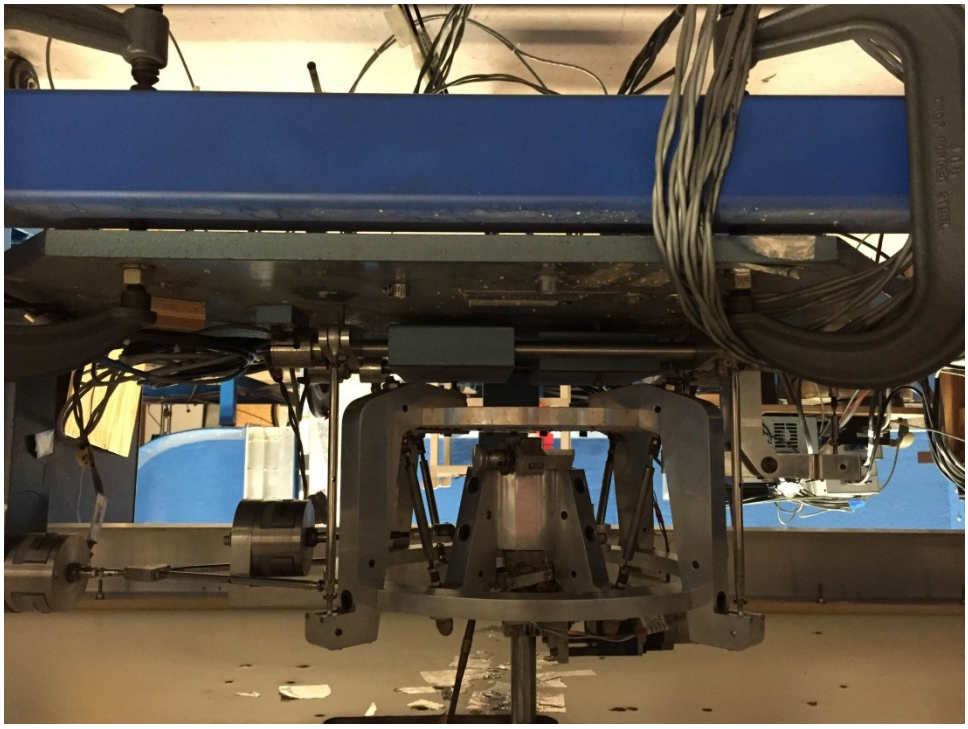

*Figure 2 - 3-Component Pyramidal Balance Under 3'x4' Wind Tunnel Test Section*

**Test Section Configuration**

Inside one of these test sections was the experimental setup used in this project. A wing of 2 ft chord, 2 ft span and a NACA 0012 shape was manufactured by Lynntech, Inc. In order to minimize wingtip effects, two end-plates were set up from the top to the bottom of the test section at each wingtip – one constructed from plywood and the other from acrylic Plexiglas. The top surface of this wing was designed so that plasma actuators could be placed at strategic spots along the surface of the wing in order to

create different configurations to be tested. This configuration is shown in Figure 3 and Figure 4.

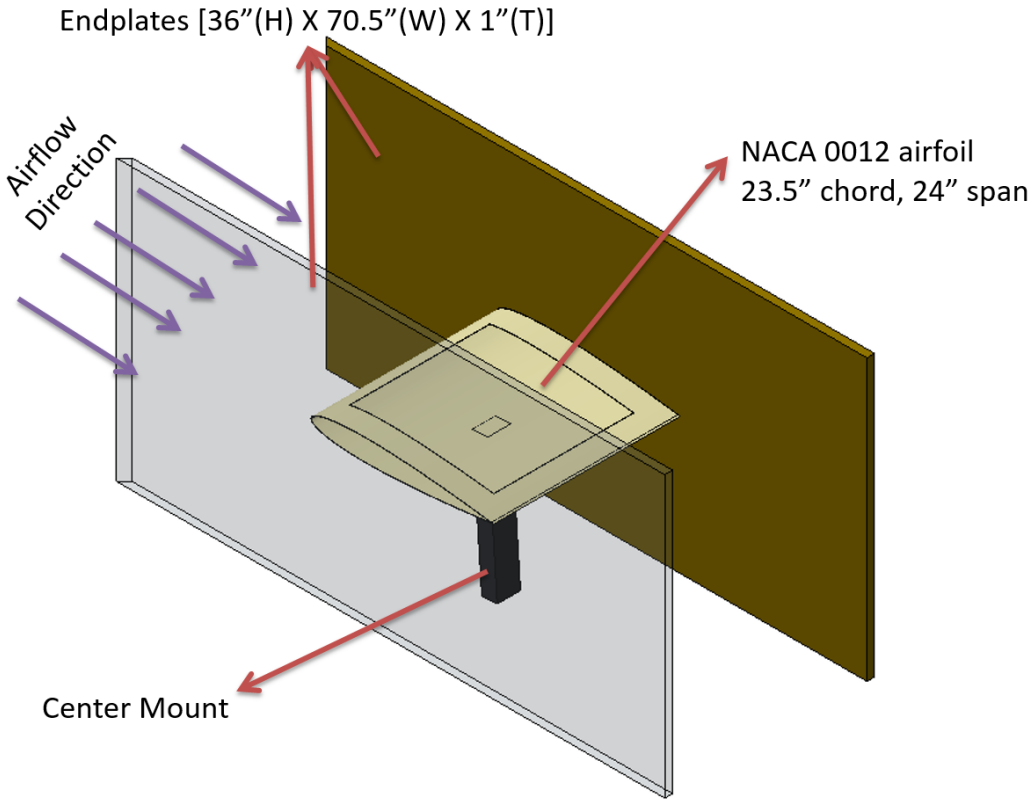


*Figure 3 - Test Section Configuration Drawing, Isometric View (Credit: Lynntech, Inc.)*

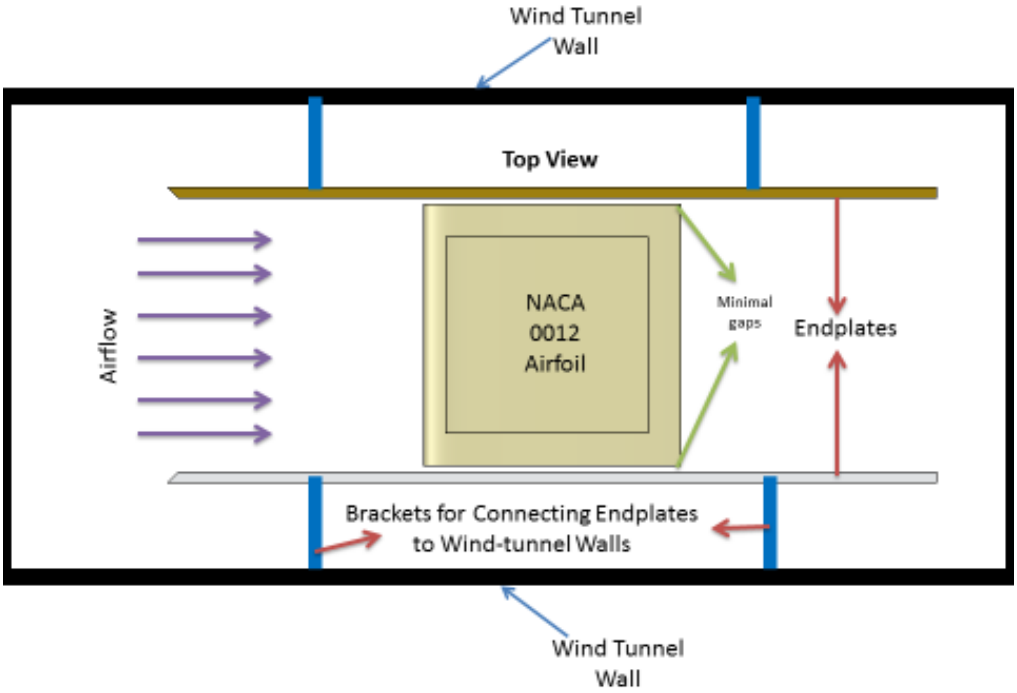


*Figure 4 - Test Section Configuration Drawing, Top View (Credit: Modified from Lynntech, Inc.)*

**Wing and Plasma Actuators**

The wing placed into the wind tunnel, designed and manufactured by Lynntech, has a NACA 0012 airfoil design with a span of 24 inches and a chord length of 23.5 inches in order to meet the target $Re_c$ of 1.6 million. Note that all further dimensions having to do with the wing and plasma actuators will be non-dimensionalized by the chord length c. This wing had a hollow construction of an ABS plastic core for the mounting of the plasma actuators with the remainder of the filling being constructed from foam. The outer surface of the wing was a smooth plastic which could be modified to fit different configurations of plasma actuators.

Within the 3-D printed core section was a 7x7 grid of slots for plasma actuators. Tests with up to seven plasma actuators at once were conducted, with other tests having as few as three. The grid starts at 0.19c in the span-wise direction and 0.3c in the stream-wise direction. The spacing of this grid was 0.106c in the span-wise direction and 0.128c in the stream-wise direction. Figure 5 is a photograph of the wing before plasma actuators were installed.

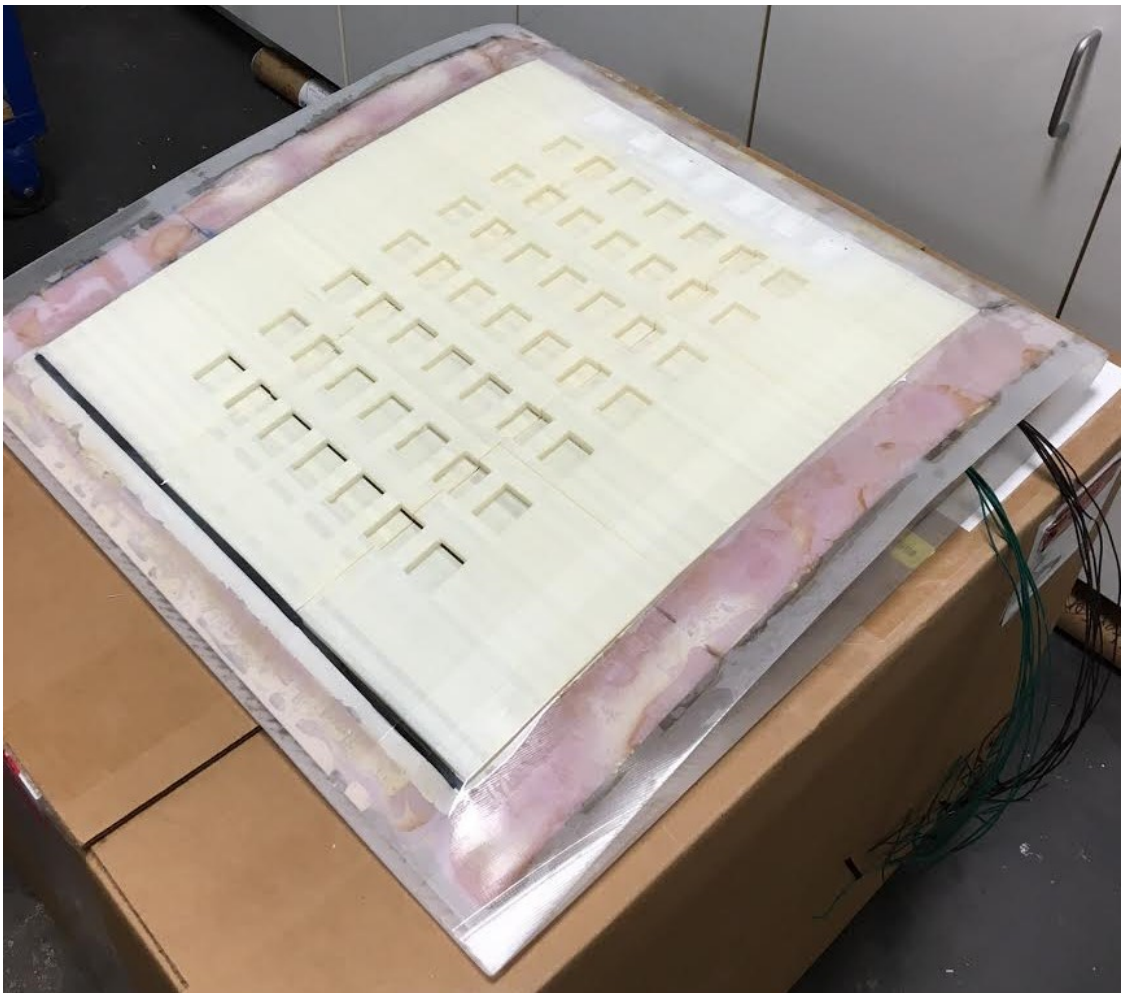

*Figure 5 - NACA 0012 Wing Used for Testing (No Plasma Actuators)*

The plasma actuators when engaged fire a small jet of plasma from a slot in the wing surface into the flow. These actuators were simultaneously pulsed at a low frequency for boundary layer measurements and at low, medium, and high frequencies for overall drag measurements.

**Constant Temperature Anemometry System**

Because of their low thermal mass, hot wires and hot films are a preferred method of taking high-fidelity and high-frequency velocity measurements in wind tunnel testing environments. Their fragility and complication in operation (at least for older systems), however, require certain care in order to conduct a successful test.

To take these velocity measurements, an IFA 300 CTA system (S/N 577) was used, along with a TSI Model 1201 probe mounted in a probe support. Figure 6 shows the dimensions of the Model 1201 probe. The hot film bridge has a thickness of 50.8 μm [14]. These were connected using a standard BNC cable. The IFA 300 is operated using proprietary software installed computer running the Windows 98 operating system. This software may be used in order to perform full calibration and data acquisition, but advances in data acquisition allow for faster operation using a separate USB DAQ card. One IFA 300 cabinet can support up to 8 channels of anemometry with onboard signal conditioning along with a thermocouple channel, although in this experiment only 1 anemometry channel was used. The IFA operates by keeping the probe bridge (hot wire or hot film) at a constant temperature. As a fluid passes over the sensor, the amplifier adjusts the voltage in order to keep the bridge at a constant temperature.

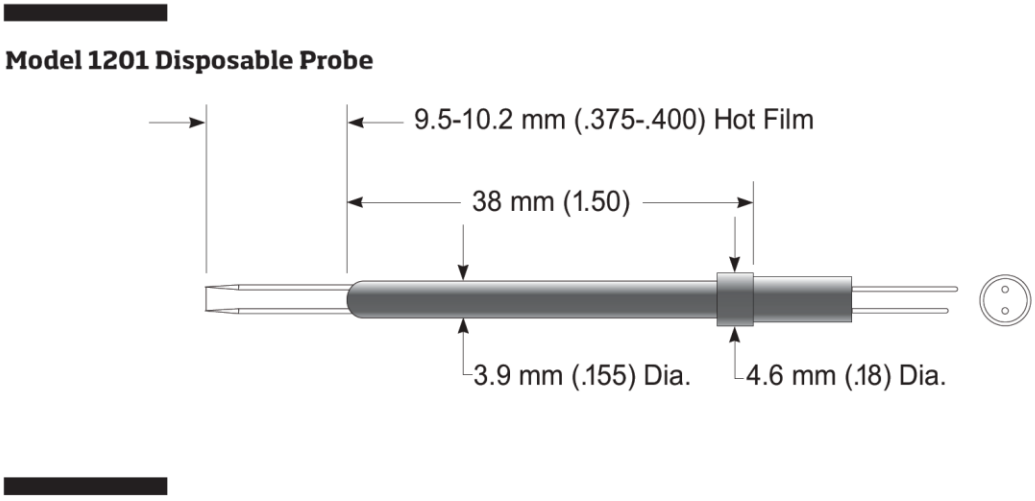


*Figure 6 - TSI Model 1201 Hot Film Probe (Credit: TSI)*

The TSI Model 1201 probe was chosen mostly for its relatively high durability and low cost compared to other hot wire probes. The bridge is a 0.05 mm diameter hot film at a sensor length of 1.0 mm. Due to one probe breaking due to an arc from a plasma actuator, two probes were used during testing – S/N 43-43 and 44-44. For this experiment, an operating resistance of 8.58Ω was used for each probe and velocity-voltage conversion was found in the freestream using the wind tunnel's pitot tube as a reference velocity for each point in the calibration. The calibration procedure was as follows:

1. Tip of hot film probe positioned 4-5 inches above and forward of the mounted wing.
2. Starting with the wind tunnel turned off, the IFA-300 was booted up and the IFA software executed.

3. IFA software was put into calibration mode to activate the anemometer so that it began to maintain a constant temperature bridge.
4. Three 2-second voltage measurements at 10kHz were recorded at 0 m/s
5. The wind tunnel was turned on.
6. The wind tunnel was brought to the next velocity point using the installed anemometer.
7. Three 2-second voltage measurements at 10kHz were recorded
8. Steps 6 and 7 were repeated for each velocity
9. For each measurement, voltage was averaged over the window
10. Average voltages were plotted vs. velocity at each voltage to form a calibration curve

Although tests were conducted using two different probes, data presented in this thesis used only S/N 44-44, and thus this calibration will be the only one presented. In a 66-point calibration using 3 windows at 22 different velocities in the wind tunnel freestream, the following calibration curve was constructed, as shown in Figure 7.

This calibration curve is constructed using a cubic polynomial regression. The $R^2$ value of 0.9997 indicates extremely good agreement with a cubic fit, especially given the large number of points used in the calibration. Furthermore, a fortuitous result of this calibration is that any electromagnetic interference experienced would have a minimized effect in the low-velocity regions in the near-wall area of interest for ascertaining the shear stress.

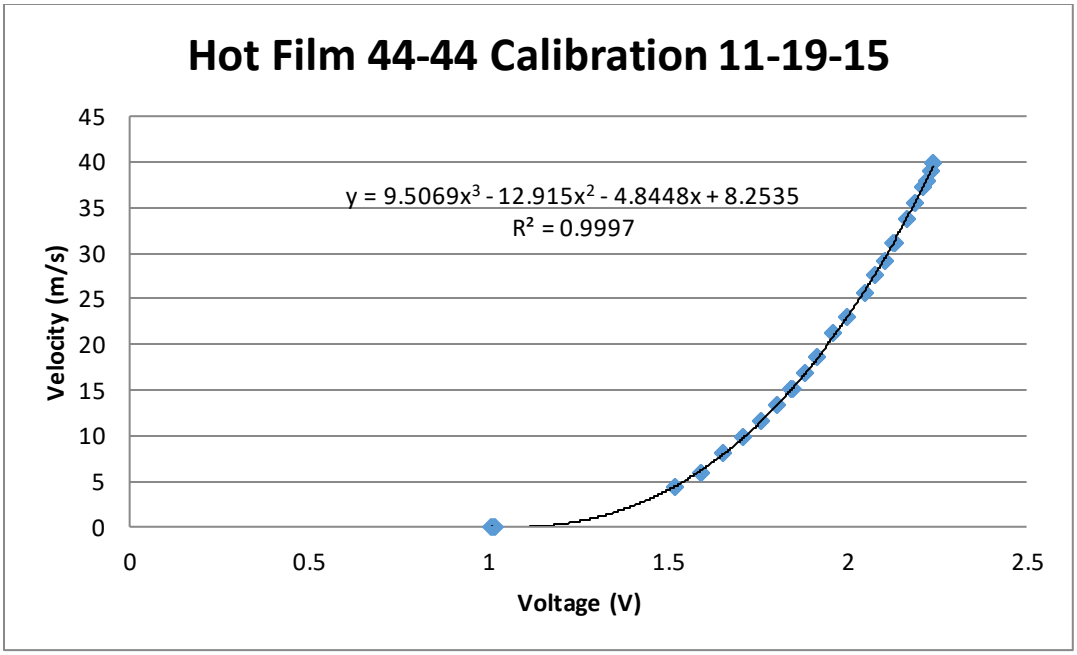


*Figure 7 - Calibration Curve for Hot Film Probe S/N 44-44*

**Data Acquisition Procedure**

Voltages from both the IFA anemometer and the pyramidal balance underneath the wind tunnel test section were acquired using a National Instruments USB-6211 DAQ card and sampled using the MATLAB Data Acquisition Toolbox.

Output voltage from the IFA 300 may be acquired as an output and correlated to flow velocity normal to the length dimension of the probe bridge. In this experiment, output voltage from the IFA cabinet was routed via a BNC cable into the analog input on the NI DAQ card and sampled by MATLAB at 10kHz at 20 kilosamples per test point.

Similarly, output voltage from the drag axis of the pyramidal balance was acquired using the NI DAQ card and sampled by MATLAB at 10kHz at 20 kilosamples per test point. This sampling rate turned out to be much faster than the response time of

the balance, and thus gave very flat values across the sample time. For the measurement of both values, electromagnetic interference was taken into account.

**Boundary Layer Measurements**

The majority of test points involved the mapping of boundary layer profiles at various locations on the wing of the airfoil with plasma actuators mounted in two different configurations. The first configuration used plasma actuators mounted parallel to the span of the wing, while the second mounted actuators in a 45-degree diagonal line from the front-left portion of the top surface of the wing to the lower-right

Using the wind tunnel test section's integral 3D traversing system (equipped with precision lead screws), the hot film probe was moved into the appropriate span-wise and stream-wise position for each test point. Each of these positions on the two axes was marked along the traversing axes for later reference. The operation wall-normal axis of the traverse involved a bit more precision since it would be the only direction manipulated for each boundary layer measurement.

A degree dial was used to make precise movements in the wall-normal direction, corresponding to 0.0749mm (74.9 microns) of travel per 5-degree rotation. The other two axes had lead screws of the same pitch, and travel was measured using a caliper and markings along the edges of the traversing scale. After a consistent lag in response while changing travel direction was noticed during testing, a Fowler-Sylvac depth gauge was mounted as a reliable measurement reference with precision of 0.001mm. Once this lag was determined to correspond to a certain number of degrees, this conversion was

applied to all previous tests to provide an accurate measure of distance from the surface of the wing. A photograph of this is shown in Figure 8.

For each test point, a consistent approach to taking a boundary layer measurement was followed. First, with the probe in the freestream, the wind tunnel was turned on and brought to the target velocity with the plasma actuators turned off. The baseline measurement of the freestream velocity as well as the reading on the depth gauge was recorded. The traverse was then lowered by a callout of a certain number of degrees corresponding to some physical distance in the wall-normal direction. A reading of the new depth and velocity measurement was recorded, continuing until the velocity started to decrease, signaling the beginning of the boundary layer. Subsequent movements downward were in increasingly smaller increments, taking velocity and position measurements until the hot film was as close to the surface as possible without contact. This gap distance was incredibly small, and measured values of velocity were as low as ~10% of the freestream, in an effort to ensure a representative profile of the boundary layer was captured. After an examination of the probe dimensions, it was determined that the closest distance to the surface at each point was 0.055mm due to the thickness of the prongs which held the hot film [13].

Once this profile was recorded, the plasma actuators were turned on at a desired frequency. The hot film probe was then used to capture the boundary layer velocity profile in a similar manner, moving away from the wall of the wing until it reached the freestream. This procedure was repeated at multiple test points and multiple times at some test points which showed interesting boundary layer behavior until all the

boundary layers at all desired test points were recorded. A photograph of the probe during one set of measurements is shown in Figure 8 below.

*Figure 8 - Photograph of Boundary Layer Measurements*

By comparing the slope of the near-wall velocity for the baseline measurement and with the plasma actuators firing, it is possible to compare the local skin-friction drag on the wing. In order to achieve a consistent approach for comparison with results reported by Lynntech, the value of $\tau_w$ was calculated by taking the slope of the nearest-wall point in each boundary layer (in this case $y/\delta < 0.01$ where possible) and the wall condition (0 m/s, y = 0 mm). The validity of this measurement will be discussed further in the next section under *Error Analysis*. After examination of the results and the

variance in the probe position from the wall, these near-wall measurements were compared with an analysis of log-layer behavior for comparison and validation.

**Direct Wing Drag Measurements**

After recording boundary layer measurements, an attempt to demonstrate a reduction in overall drag was attempted using the pyramidal balance attached to the sting upon which the wing was mounted. This pyramidal balance is capable of measuring lift, drag, and pitching moment, but for the purposes of this experiment only the drag axis was used. All drag measurements were taken with plasma actuators in the diagonal configuration.

First, the drag axis was calibrated by using a pulley system and suspended known weights in order to establish a calibration curve for the balance. Starting with zero weight and moving up to about 30 N of force by adding incremental known weights, a linear fit was established. This fit was used to convert the output voltage of the balance into a force measurement, and may be found in Figure 9. All points in the ten-point force calibration may be found in Table in Appendix A.

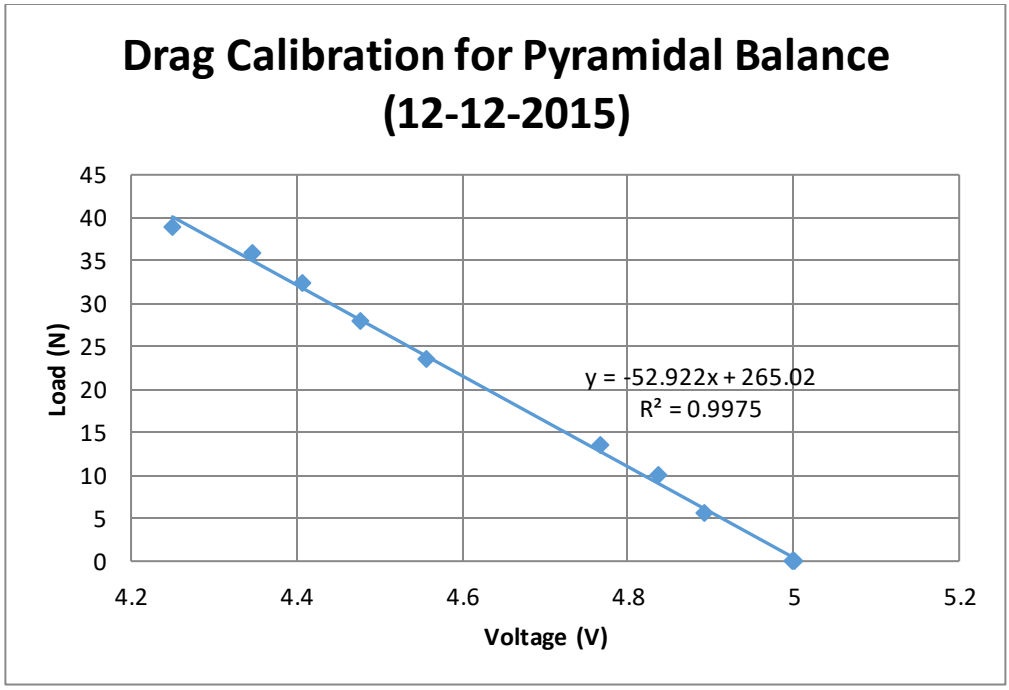


*Figure 9 - Calibration Curve for Test Section Pyramidal Balance Drag Axis*

In order to determine the effects of electromagnetic interference from the plasma actuators, zero-load readings were taken with the wind tunnel turned off. Several voltage readings from the pyramidal balance were taken with the plasma actuators turned off, then pulsed at low, medium, and high frequencies. Then, the wind tunnel was brought to 40m/s freestream and a baseline drag measurement was taken with the plasma actuators turned off. Then the plasma actuators were turned on and set to several different frequencies. Several Different combinations of plasma actuators were used, and are indicated in the Results and Discussion section. Each of these different test conditions was repeated several times to increase certainty in the results. Voltage readings were recorded and converted to drag force for each test condition.

## RESULTS AND DISCUSSION*

### Boundary Layer Measurements

Boundary layer measurements taken indicated some signs of both local and overall drag reduction. These changes in drag were highly-dependent upon location, plasma actuator configuration, and plasma actuator frequency, but drag reductions were demonstrated in several different locations. However, several general trends were observed for most locations in the area of influence of a plasma actuator. It should be emphasized that the mechanism for any observed drag reduction is merely hypothesized to be due to a span-wise traveling wave and that several other flow phenomena could explain this reduction, warranting further investigation in future studies.

In the proceeding sub-subsections, boundary layer velocity profiles and corresponding wall shear stress ($\tau_w$) and friction coefficient ($C_f$) are presented. Note that the height from the wall is non-dimensionalized by the boundary layer thickness $\delta$, defined as the wall-normal distance where local velocity is 99% of the freestream). The boundary layer thickness was calculated by a linear interpolation between the wall-normal locations closest to a velocity measurement equal to 99% of the freestream value. This differs for each boundary layer examined. Additionally, note the distinction between $U$, the local freestream velocity, and $U_\infty$, the tunnel freestream velocity. Because of the movement of the flow over the surface of the wing, this velocity may not be exactly equal to the tunnel freestream velocity.

* Portions of this section report data from Lynntech, Inc. *Drag Reduction through Pulsed Plasma Actuators: Phase I Final Report*, December 2015.

Thus, these plots should not be used to directly calculate wall shear stress, but are designed to show a qualitative distinction showing the average effect of the plasma actuators over the 2-second sampling window.

*Span-wise Line Configuration – Stream-wise Sweep*

The first testing configuration was the span-wise sweep with actuators evenly-spaced at 0.106c in the span-wise direction. Measurements were taken downstream of Actuator 2. Figure 10 & Figure 11 show the boundary layer profile at an x-location of 0.39c, or 0.09c downstream of the plasma actuator. This location shows a near-wall low-

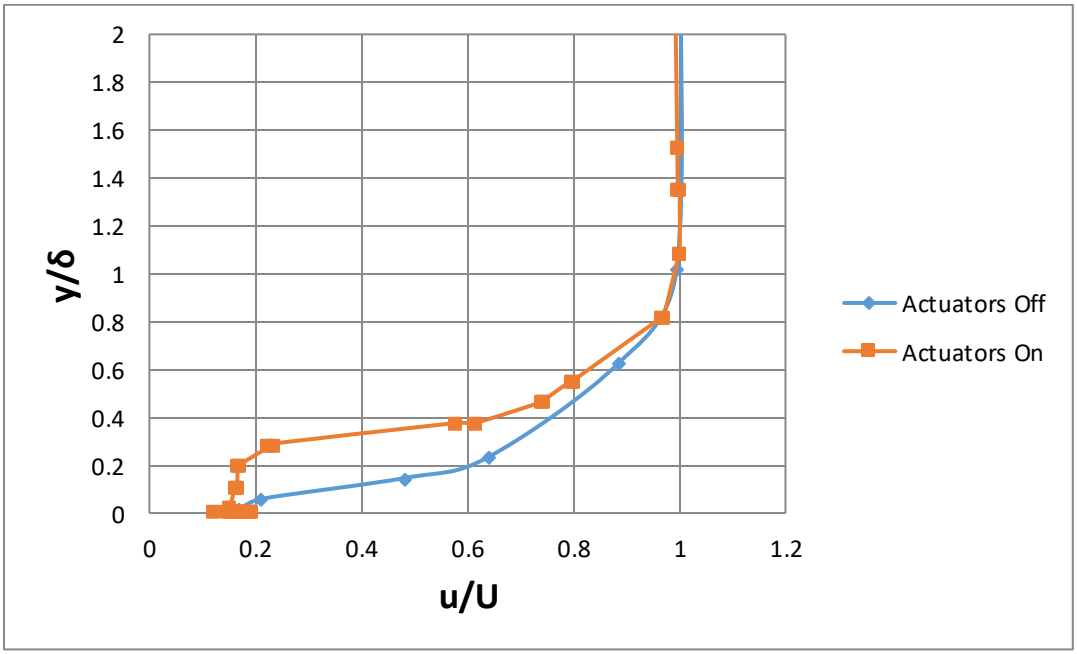


*Figure 10 - Boundary Layer Profile at 0.39c, 0.09c Downstream from Actuator 2*

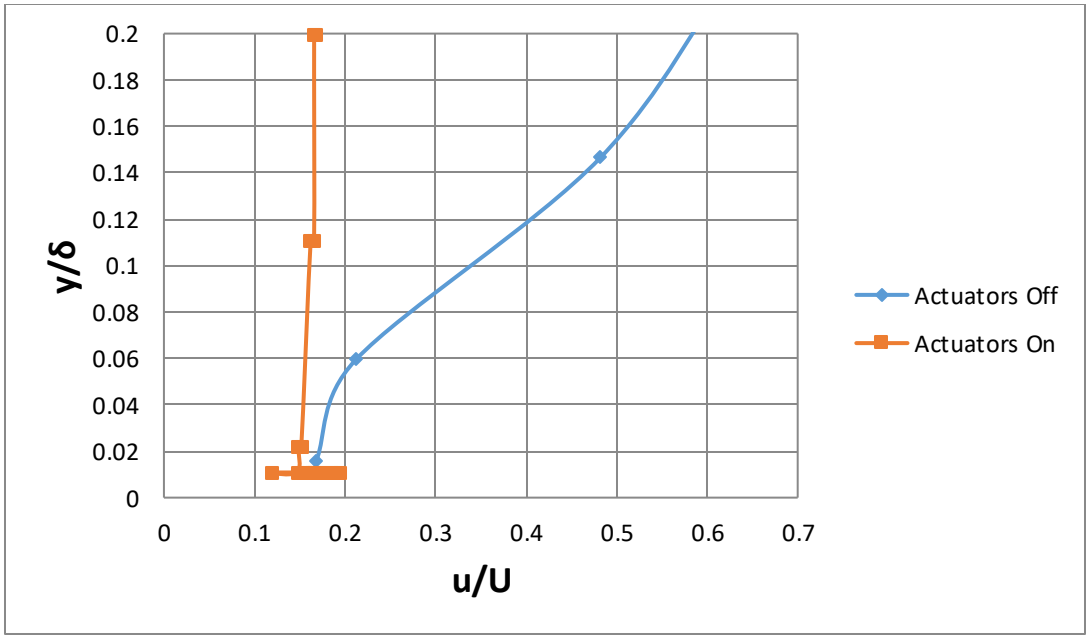


*Figure 11 - Boundary Layer Profile at 0.39c, 0.09c Downstream from Actuator 2 (Close to Wall)*

-velocity region when the plasma actuators are engaged. Two sweeps were taken at 0.43c, with boundary layer profiles shown in Figure 12 and Figure 13. The near-wall velocity deficit is still qualitatively evident in both profiles with the plasma actuators on, but differences in the near-wall velocity in the nominal boundary layer profiles lead to disagreement as to whether drag was reduced or increased.

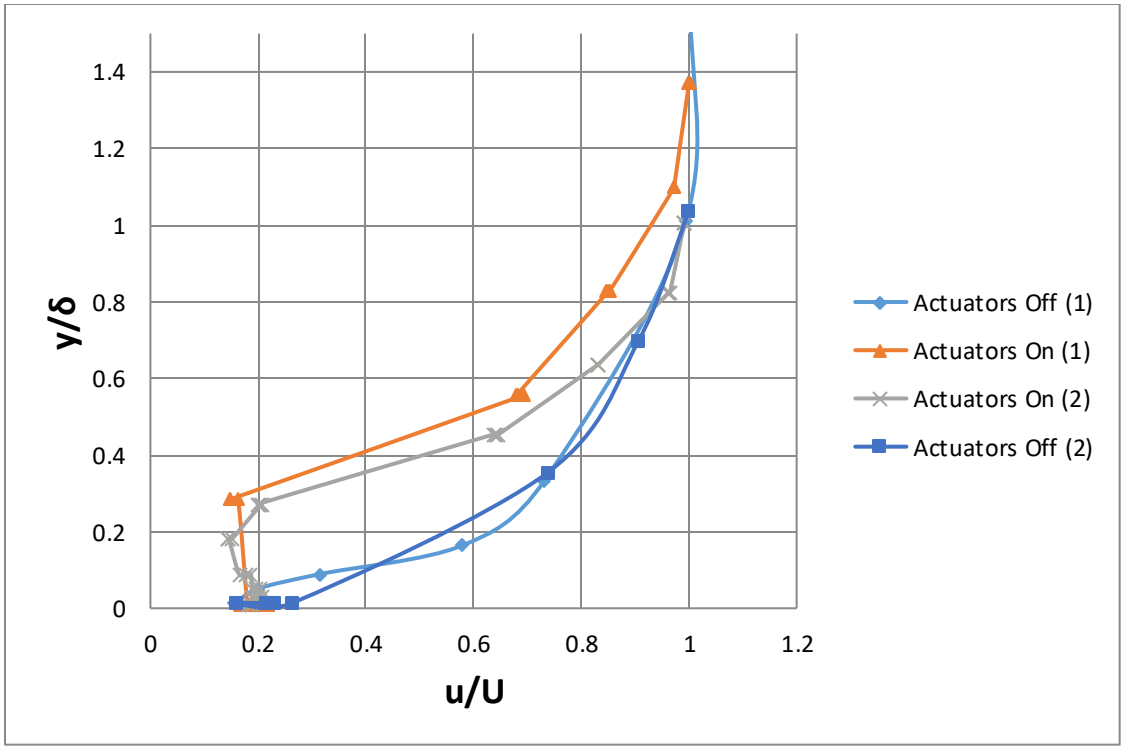


*Figure 12 - Boundary Layer Profile at 0.43c, 0.13c Downstream from Actuator 2*

Proceeding further still downstream, the boundary layer behavior of profiles at 0.53c show similar behavior to those observed very close to the actuator. Figure 14 and Figure 15 show behavior, indicative of lower wall stress. The final location sampled in the stream-wise sweep was at a location of 0.61c. This location showed a larger wall stress when the actuators on, like the 0.43c location. Unlike the 0.43c location, however, the 0.61c location did not show a near-wall velocity deficit region in its boundary layer behavior this is shown in Figure 16 and Figure 17.

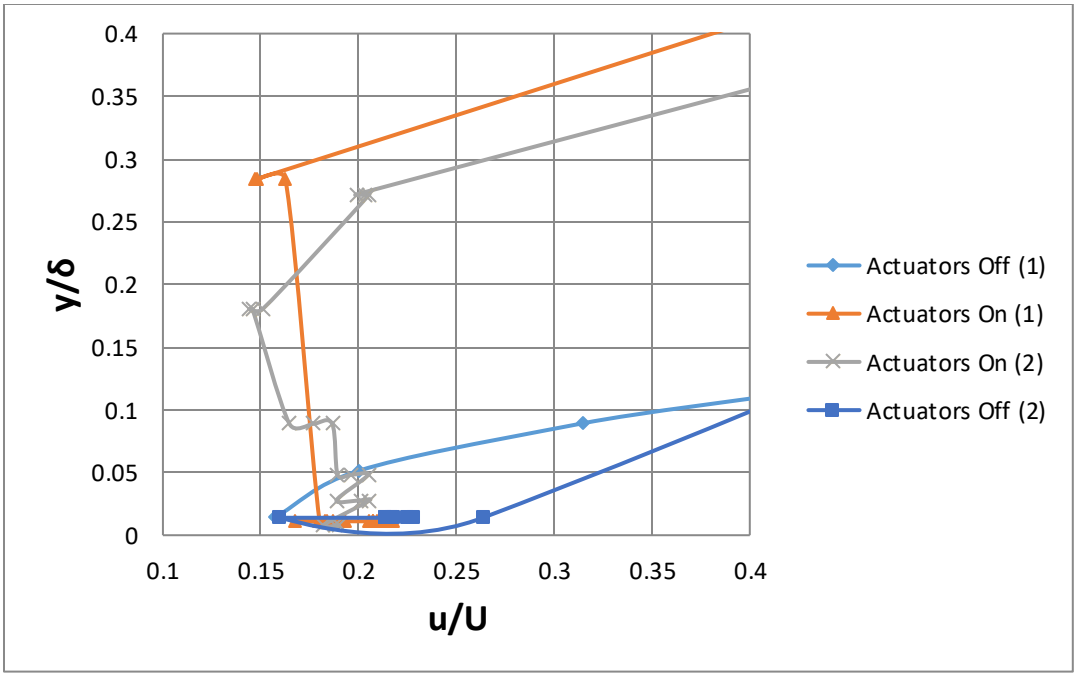


*Figure 13 - Boundary Layer Profile at 0.43c, 0.13c Downstream from Actuator 2 (Close to Wall)*

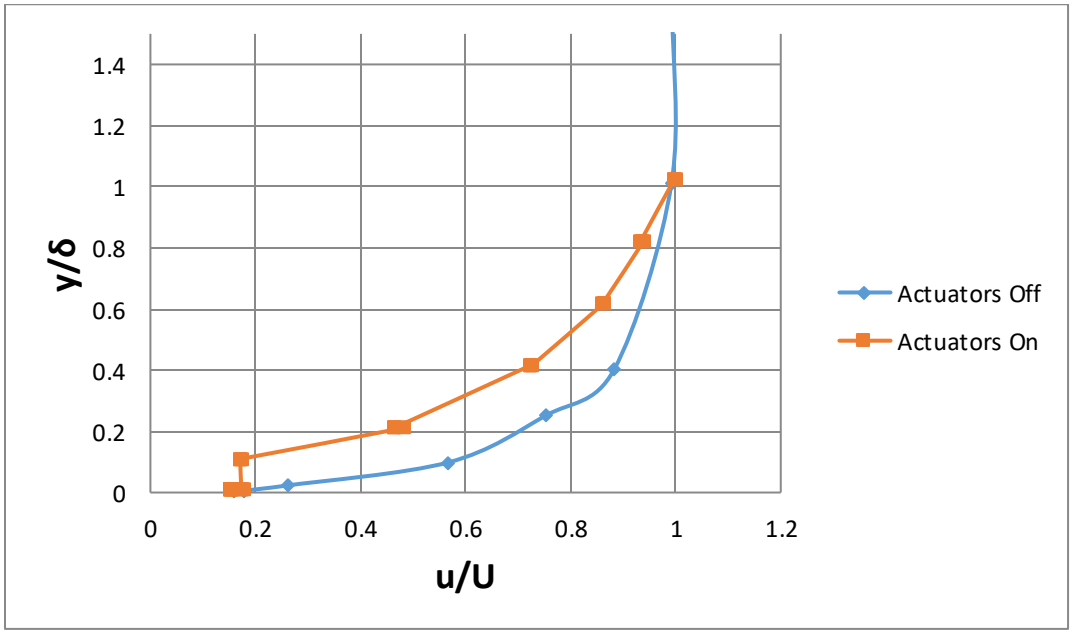


*Figure 14 - Boundary Layer Profile at 0.53c, 0.22c Downstream from Actuator 2*

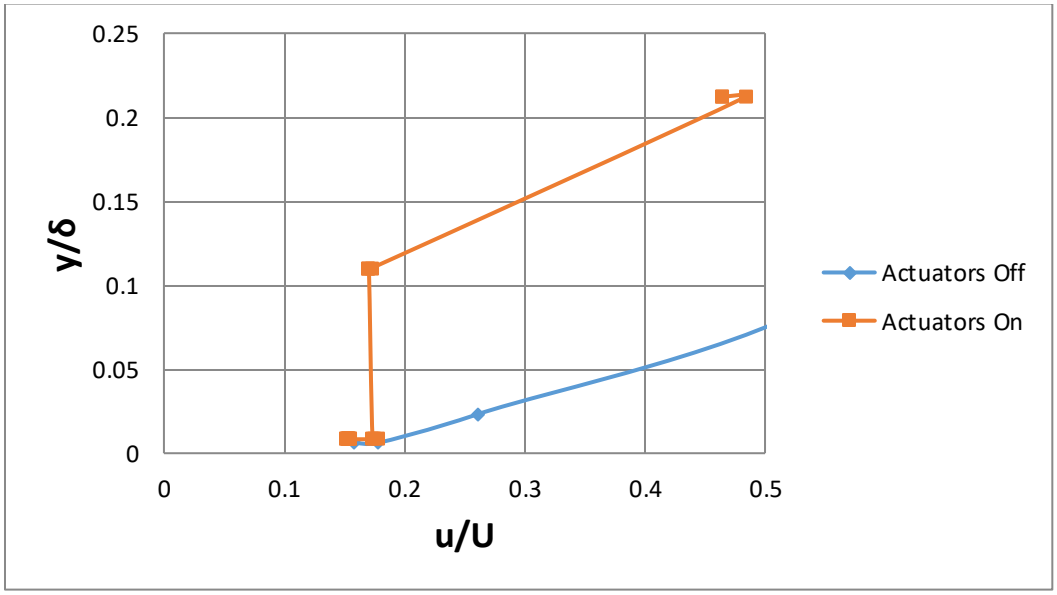


*Figure 15 - Boundary Layer Profile at 0.53c, 0.22c Downstream from Actuator 2 (Close to Wall)*

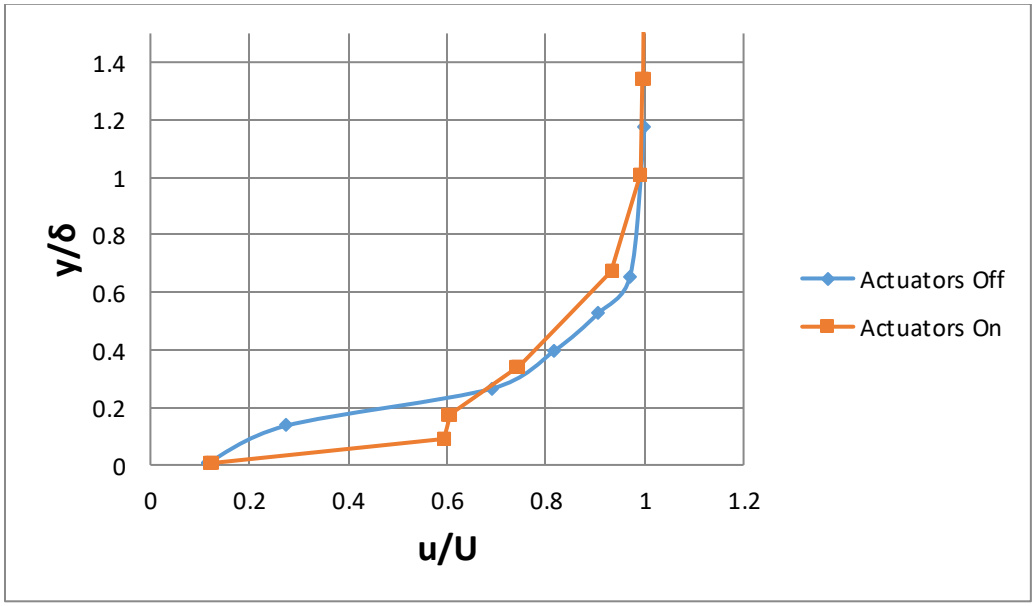


*Figure 16 - Boundary Layer Profile at 0.61c, 0.31c Downstream from Actuator 2*

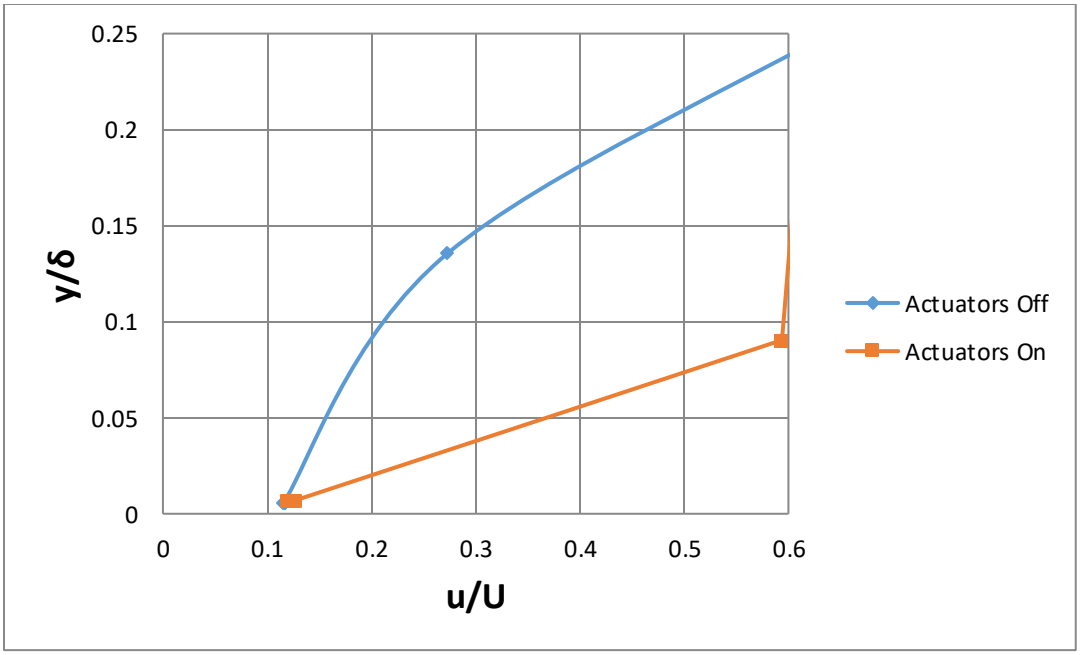


*Figure 17 - Boundary Layer Profile at 0.61c, 0.31c Downstream from Actuator 2 (Close to Wall)*

*Table 1 - Wall Shear Stress and Friction Coefficient Comparisons at Different Stream-Wise Locations*

| | X-Location | | | | |
|---|---|---|---|---|---|
| | **0.39c** | **0.43c (1)** | **0.43c (2)** | **0.53c** | **0.61c** |
| **Actuators Off** | | | | | |
| $\tau_w$ (Pa) | 2.3769 | 2.3619 | 3.5087 | 2.4780 | 1.4908 |
| $C_f$ | 0.002466 | 0.002450 | 0.003640 | 0.002571 | 0.001546 |
| **Actuators On** | | | | | |
| $\tau_w$ (Pa) | 2.2303 | 2.7177 | 2.5890 | 2.1375 | 1.6425 |
| $C_f$ | 0.002314 | 0.002819 | 0.002686 | 0.002217 | 0.001704 |
| **% Reduction** | 6.17 | -15.06 | 26.21 | 13.74 | -10.17 |

A summary of the calculated values for $\tau_w$ and $C_f$ for this plasma actuator configuration are presented in Table 1. These results indicate the presence of modest drag reduction in two locations in the stream-wise direction along with a local increase in drag in one region. The results for the 0.43c location show inconsistent results based on two separate sweeps and are therefore a subject of dispute with results reported by Lynntech for the same location. This discrepancy will be discussed later in this section.

*Diagonal Line Configuration – Span-wise Sweep*

The second testing configuration examined was a span-wise sweep just behind plasma actuator 5, which was located in the fifth row and fifth column in the grid of plasma actuator slots in the wing. Other actuators were similarly placed at (1,1), (2,2), (3,3), (4,4), (6,6), and (7,7) locations.

Starting between actuators 5 and 6, in the span-wise direction and 0.021c behind actuator 5 in the stream-wise direction and moving starboard in the span-wise direction, boundary layer measurements were taken at several locations to examine the span-wise extent of plasma actuator effects on the boundary layer.

Figure 18 and Figure 19 show the boundary layer profiles at 0.83c, 0.04c right of actuator 5. As noted in stream-wise sweep above, the plasma actuators created a low-velocity region close to the wall, which suggests reduced wall shear stress and therefore reduced skin-friction drag. Similar behavior is shown at other span-wise locations. Figure 20 and Figure 21show the boundary layer profiles for a span-wise move of 0.064c starboard of actuator 5 at the same chord location as the other tests in this set (0.83c, just downstream of actuator 5). Figure 22 and Figure 23 show similar behavior, with a

reduced near-wall velocity deficit, which is consistent with intuition considering the movement away from the influence of any plasma actuator (excepting any upstream effects from actuator 6 downstream).

The effect of the actuators on drag at a further span-wise location, 0.149c starboard, is complicated by inconsistent measurements of the bottom part of the nominal boundary layer (actuators off). These profiles are shown in Figure 24 and Figure 25. In one case, an increase in stream-wise velocity near the wall is measured, which results in a larger calculated wall stress. A second case shows a qualitative behavior more consistent with other nominal boundary layers in this set, although its calculated wall stress was lower than the average of the entire set. The behavior of the boundary layer with plasma actuators on is qualitatively consistent with other results in the set and has a resultant wall stress value between the two measured nominal values. This makes conclusions difficult to draw, and will be discussed in more detail later in this section.

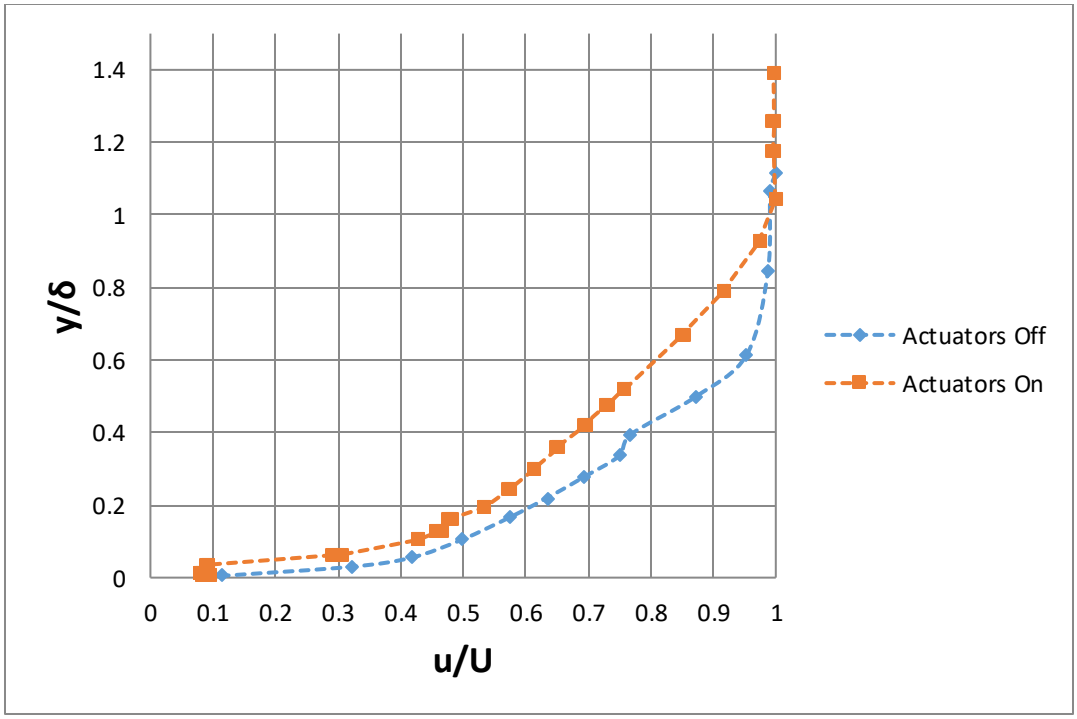


*Figure 18 - Boundary Layer Profile at 0.83c, 0.04c Right of Actuator 5*

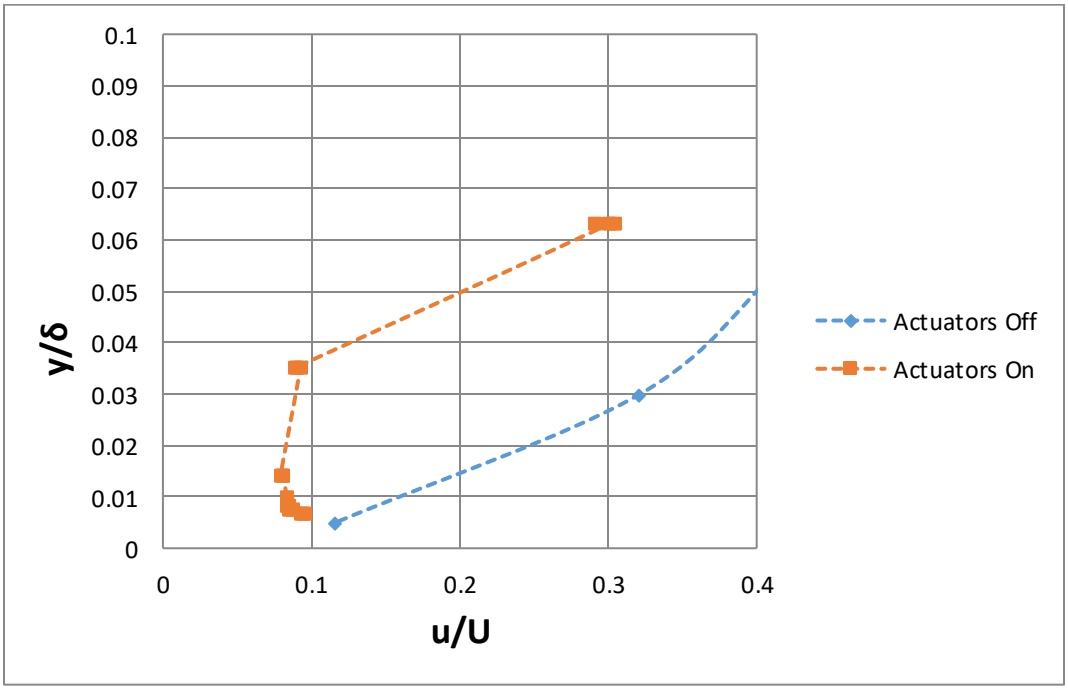


*Figure 19 - Boundary Layer Profile at 0.83c, 0.04c Right of Actuator 5, Close to Surface*

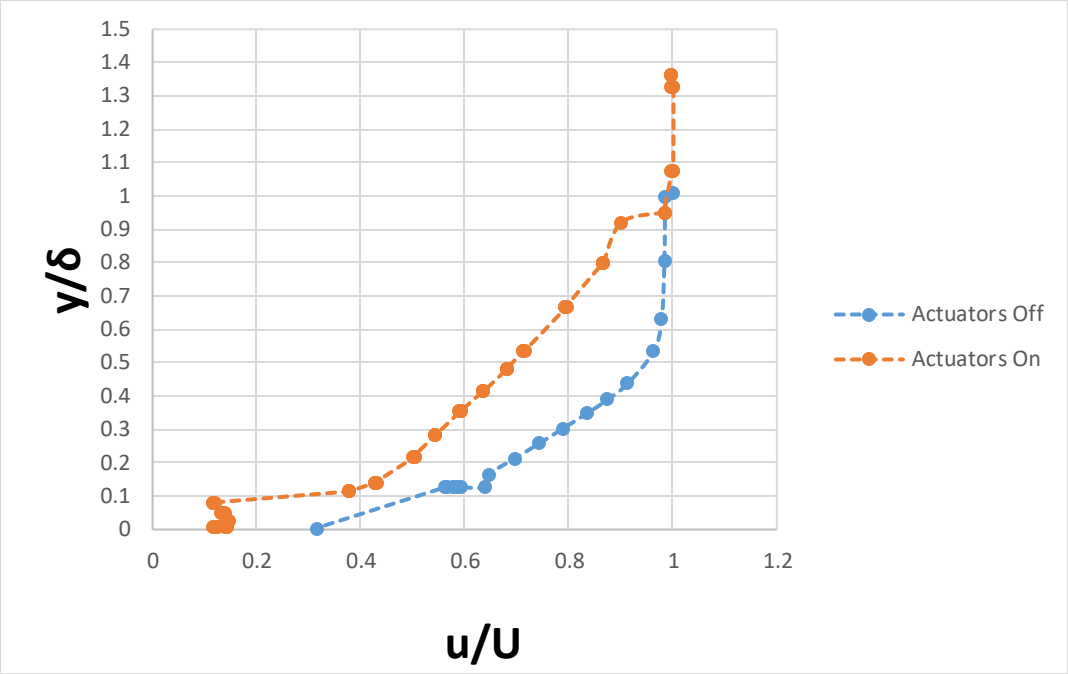


*Figure 20- Boundary Layer Profile at 0.83c, 0.064c Right of Actuator 5*

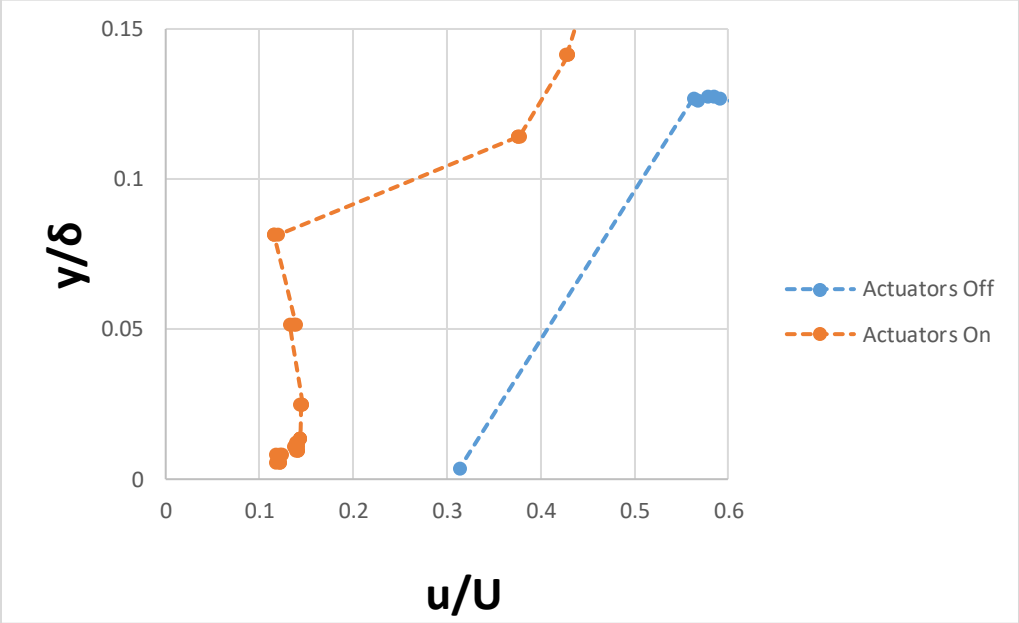


*Figure 21 - Boundary Layer Profile at 0.83c, 0.064c Right of Actuator 5, Close to Surface*

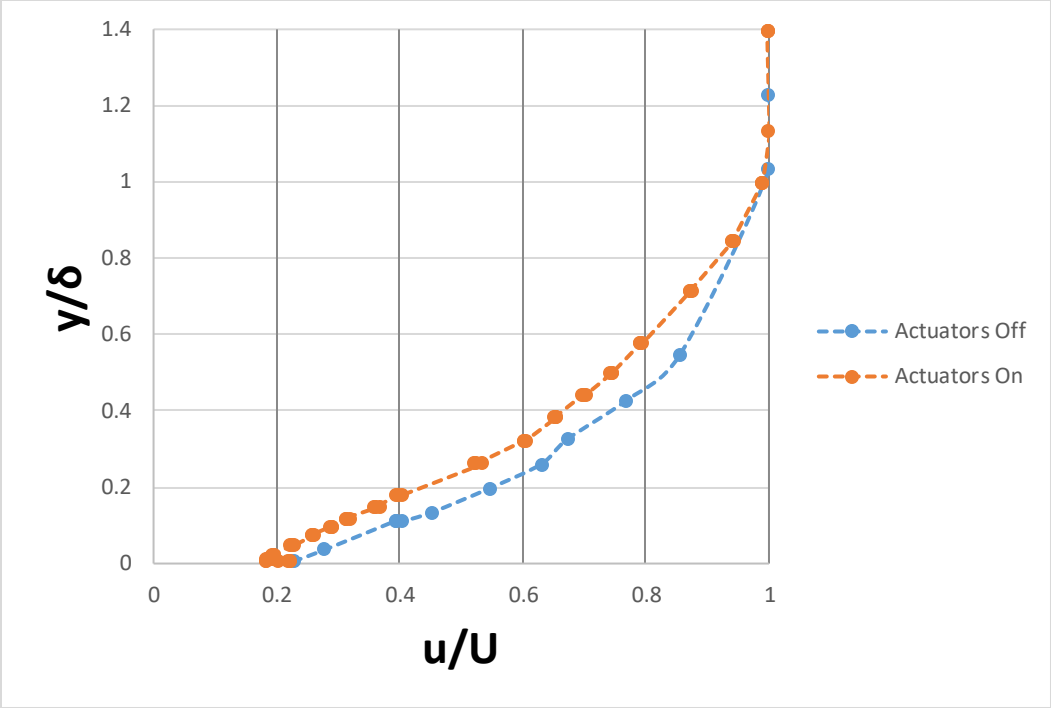


*Figure 22 - Boundary Layer Profile at 0.83c, 0.106c Right of Actuator 5*

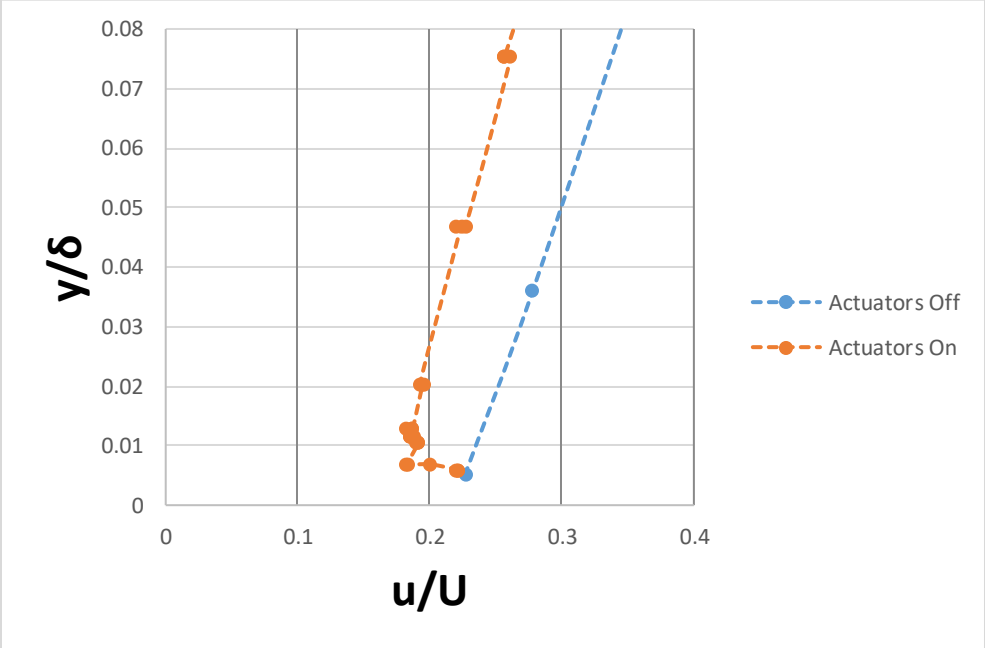


*Figure 23 - Boundary Layer Profile at 0.83c, 0.106c Right of Actuator 5, Close to Surface*

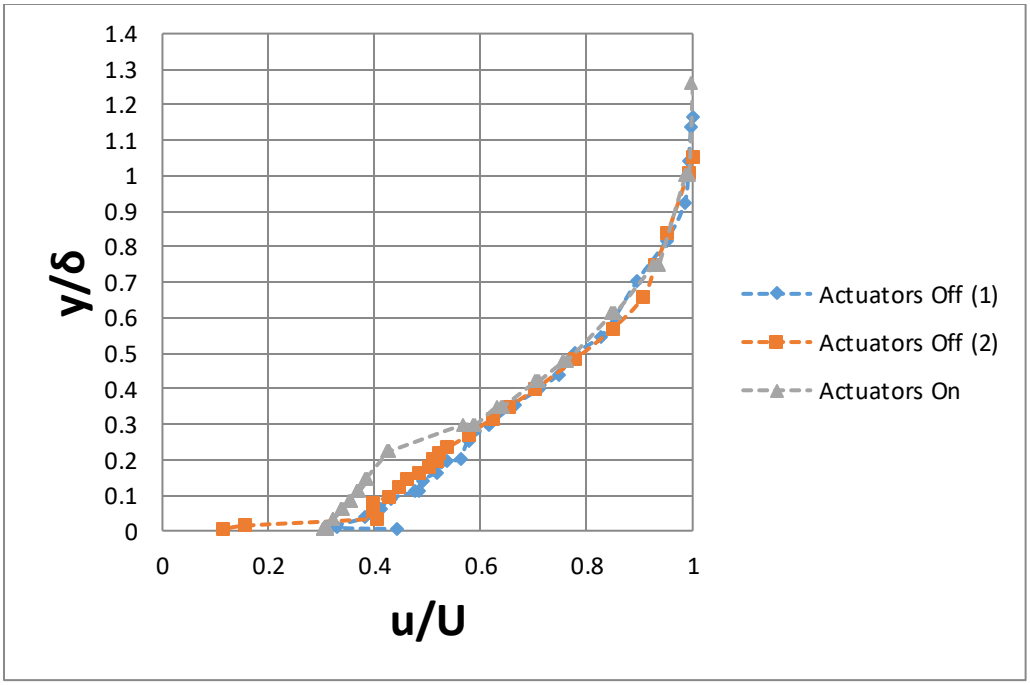


*Figure 24 - Boundary Layer Profile at 0.83c, 0.149c Right of Actuator 5*

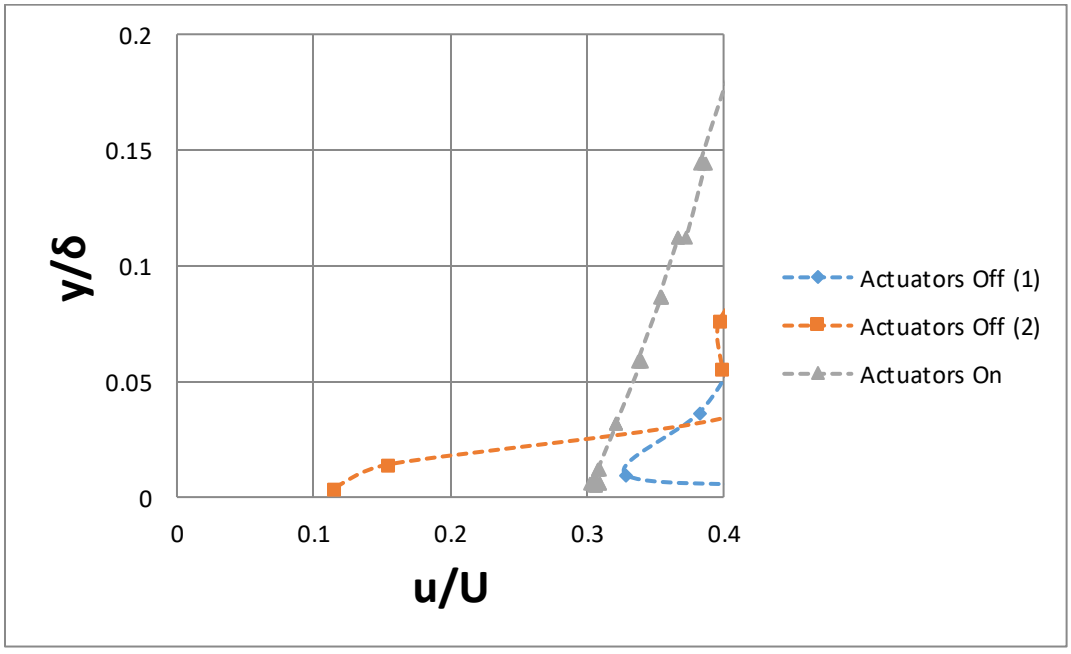


*Figure 25 - Boundary Layer Profile at 0.83c, 0.149c Right of Actuator 5, Close to Surface*

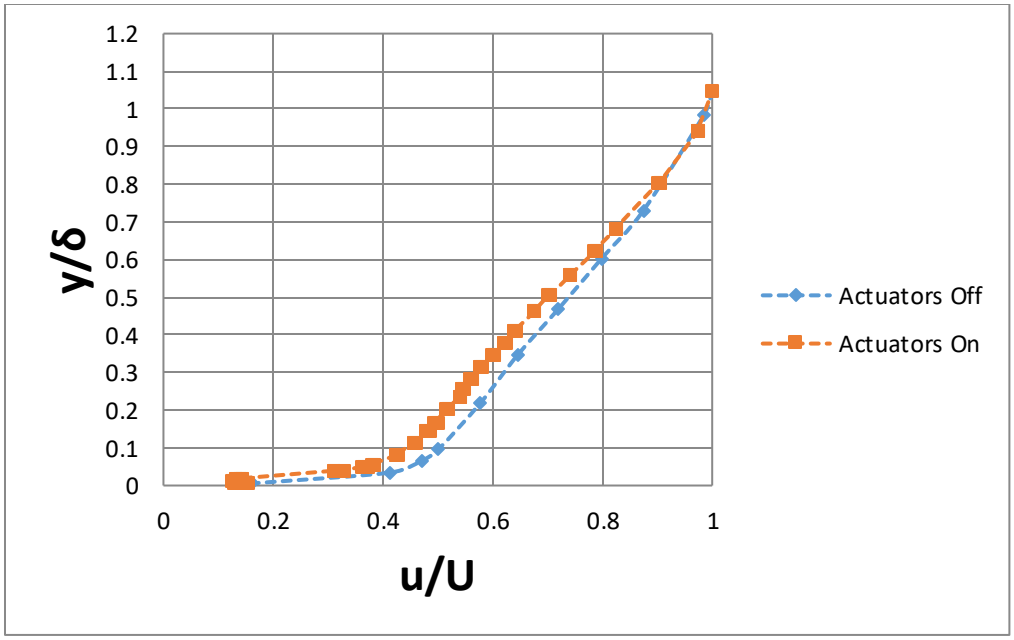


*Figure 26 - Boundary Layer Profile at 0.83c, 0.17c Right of Actuator 5*

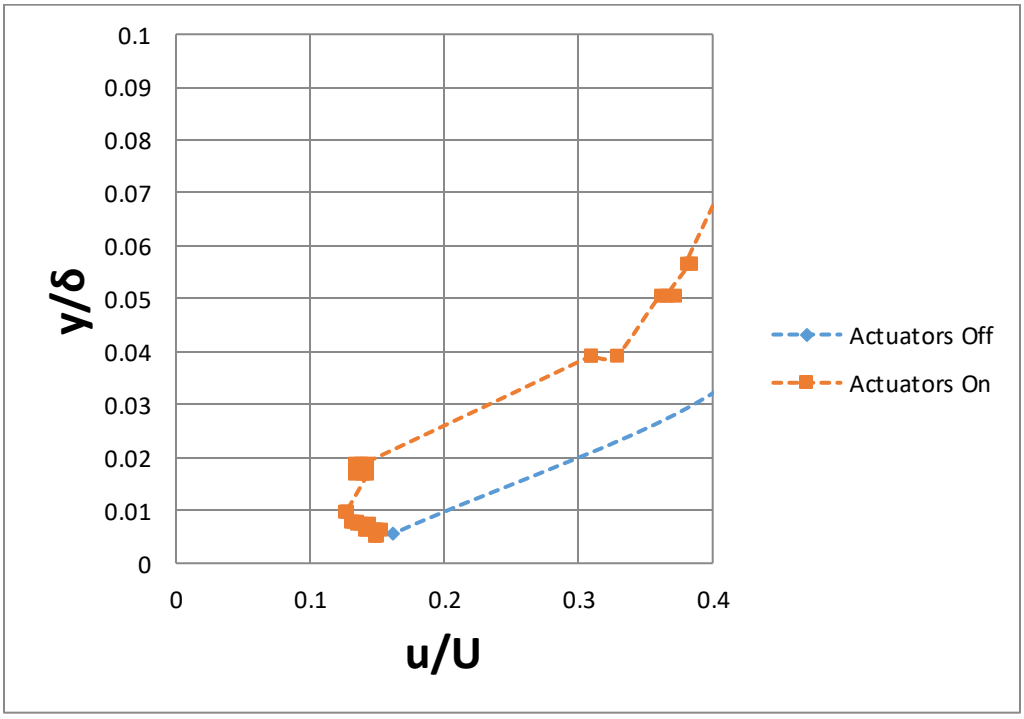


*Figure 27 - Boundary Layer Profile at 0.83c, 0.17c Right of Actuator 5, Close to Surface*

*Table 2 - Wall Shear Stress and Friction Coefficient Comparison for Different Span-Wise Locations*

| | Spanwise Location (Right of Actuator 5) | | | | | | |
|---|---|---|---|---|---|---|---|
| | **0.043c** | **0.064c** | **0.106c** | **0.149c(1)** | **0.149c(2)** | **0.170c** | **Average** |
| **Actuators Off** | | | | | | | |
| $\tau_w$ (Pa) | 1.5389 | 4.3691 | 2.7571 | 5.1905 | 1.6836 | 2.1839 | 2.9539 |
| $C_f$ | 0.001596 | 0.004532 | 0.002860 | 0.005384 | 0.001747 | 0.002265 | 0.003064 |
| **Actuators On** | | | | | | | |
| $\tau_w$ (Pa) | 0.8532 | 1.4535 | 2.4727 | 4.3355 | 3.4745 | 1.9658 | |
| $C_f$ | 0.000885 | 0.001508 | 0.002565 | 0.004497 | 0.003604 | 0.002039 | |
| **% Reduction** | 44.55 | 66.73 | 10.32 | 16.47 | -106.37 | 9.99 | |

Complicating this still are boundary layer measurements at 0.17c, shown in Figure 26 and Figure 27, which show a modest decrease in wall stress while the plasma actuators are activated.

The resultant calculated $\tau_w$ and $C_f$ for this configuration are shown in Table 2. All locations in the span-wise direction show a decrease in wall stress and friction coefficient with plasma actuators pulsing with the exception of one of the nominal boundary layers for the 0.149c starboard location. Drag reductions of up to 66% were shown at a few locations, indicative of the upper-bound of the effects shown in simulations mentioned earlier in this document.

*Discussion*

In general, the plasma actuators created a near-wall low stream-wise velocity region in the vicinity of the actuator. This is consistent with the computational results observed by Du and Karniadakis. The lower velocity closer to the wall results in a

smaller calculated wall shear stress, which results in lower turbulent skin-friction drag when compared to the nominal (actuator off) boundary layer. Some locations, however, saw a higher velocity at the wall and a higher drag, while still others had inconsistent results.

Several observed phenomena would be consistent with predicted behavior from the effects of a stream-wise traveling wave, which would indicate that these plasma actuators were successful in producing this effect. Because the intensity of the plasma jet pulse would be reduced by viscous forces as it traveled in the span-wise direction, a span-wise decay in drag reduction would be expected after a certain "sweet spot" intensity was reached, which is consistent with results observed in the span-wise sweep in the diagonal line configuration. Additionally, a near-wall low-velocity region downstream of the actuators is observed, although this region could show periodic behavior depending on which of the 0.43c location sweeps are to be believed. However, in the absence of full flow-characterization and several different actuator configurations and pulse frequencies, this effect is merely a hypothesized mechanism of drag reduction.

Discrepancies in calculated drag were observed at two measured locations – one in the stream-wise sweep and one in the span-wise sweep. Since the stream-wise sweep was also independently analyzed by the Lynntech team, this point should be addressed first since it is not an internal inconsistency in measurement (which could simply be cause for further investigation), but an inconsistency in reported values. At the 0.43c location in the span-wise direction, two boundary layer profiles each were taken. One sweep in each was taken traveling down in the wall-normal direction and one was taken

traveling up in the wall-normal direction. Since there were two sweeps taken and only one was reported by Lynntech in their Phase I report [13], a closer examination of the data available was necessary. Using the plots in the report and the Data Thief III software [14], it was possible to determine with good precision the near-wall $u/U$ values used to calculate the wall stress and friction coefficient and compare these values to those in the raw data sets used for the results and analysis in this thesis.

A quick examination of these graphs show a near-wall $u/U$ of 0.22 and 0.19 for the actuators off and the actuators on, respectively. This is consistent with the nearest-wall data points for the second set of sweeps. However, there seemed to be an anomaly that took place in the second sweep with the actuators turned off (probe traveling up in the wall-normal direction). Unlike every other nominal boundary layer examined in either set of sweeps, this boundary layer has a single point in which the hot film read a much smaller velocity ($u/U = 0.14$) than anywhere else in either sweep. However, even excluding this point does not remove all disagreement between the plots, as shown below in Figure 28 and Figure 29. However, it seems that there is significant agreement, particularly in the near-wall regions, between the second sweep with both actuators on and actuators off. Further consultation with Lynntech may be necessary to determine why the second sweep was chosen and the first excluded from their report. The differences between these sweeps will be discussed in the *Error Analysis* sub-subsection below.

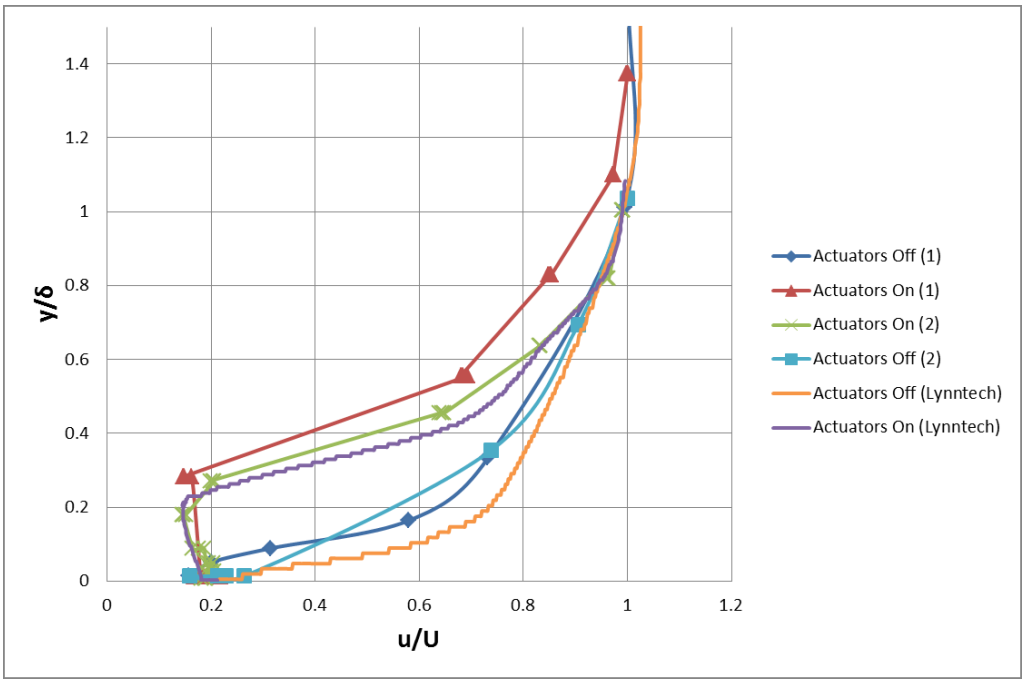


*Figure 28 - Boundary Layer Profile Comparison - Russo and Lynntech Results*

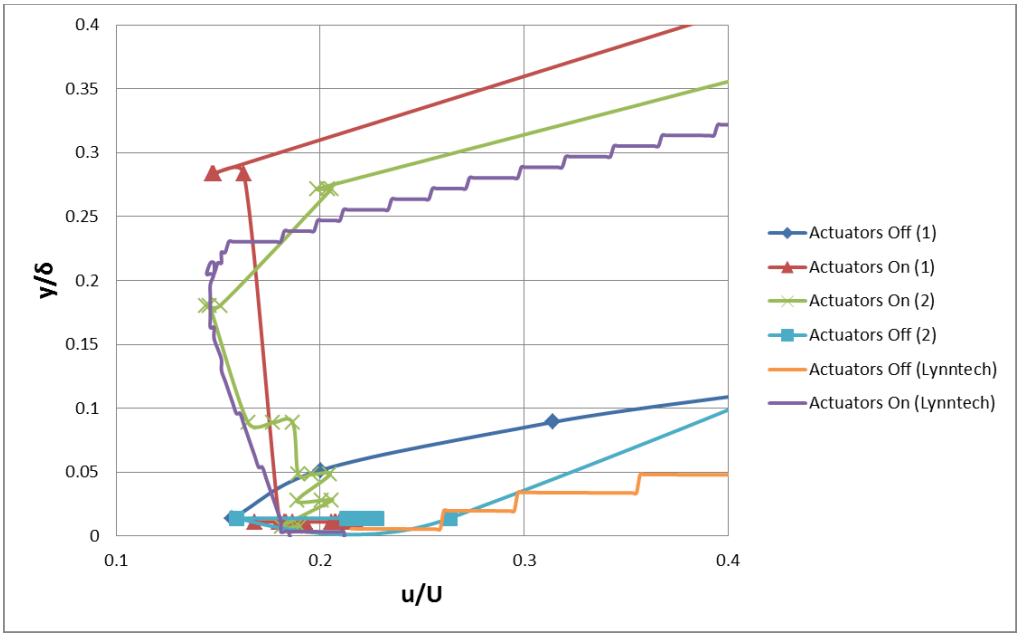


*Figure 29 - Boundary Layer Profile Comparison - Russo and Lynntech Results (Close to Wall)*

One particularly concerning result was the variance in boundary layer measurements along the span-wise direction with the actuators off. Since this is theoretically an infinite wing, span-wise properties should be identical at a given stream-wise location along the wing. However, since this is a physical system, there are sure to be some differences in the surface of the wing that could lead to slightly different values of local wall stress and friction coefficient. For example, the filler material for the plasma actuator slots is rougher than the other parts of the wing surface. Also, the covering of the plasma actuator slot grid resulted in some slight ridges running in the stream-wise direction where edges of tape met. The average value of this stream-wise location can be compared to available experimental and computational data in order to assess if these measurements, on average, were consistent with computational and experimental data for the NACA 0012 airfoil.

*Error Analysis*

At various stages during the planning, experimentation, and data analysis phases of this project, several potential sources for error in boundary layer measurements were identified. Some of these sources of error, such as the discrete thickness of the hot film probe tip, are systematic and quantifiable in nature, while others, such as errors due to tunnel heating during continuous runs, are less clear and may be mitigated somewhat by the treatment of the data.

The first source of error is a systematic error involving the nature of the velocity measurements themselves. Due to limited funding and time, the hot film chosen has a relatively large sensing area. This makes the probe more robust and less likely to break

from light contact with the model, but also makes precise measurements near the bottom of the boundary layer quite difficult. In turbulent flows, In fairness, this is an extremely difficult measurement to make no matter what kind of technique is chosen – even thinner hot wires are invasive and may change the velocity in the boundary layer as they are lowered into position. In addition, any model vibration or accidental overshoot in probe movement could cause the hot wire to contact the surface and break, which would cause delays and significant expense. Optical methods such as Particle Image Velocimetry and even point measurements such as Laser Doppler Velocimetry have similar challenges due to poor flow-following in low-velocity regions for the former and problems with laser reflections in both methods.

In particular, the wall-normal distance is significant in determining the wall stress and friction coefficient. In turbulent flows, a general rule is that wall stress must be measured within the linear sublayer, generally located at a non-dimensional wall distance $y^+ < 5$ [3], where

$$y^+ \equiv \frac{u_* y}{\nu}$$

with $y$ as the wall-normal distance from the wall, $\nu$ as the kinematic viscosity of the fluid, and $u_*$ as a so-called friction velocity of nearest the wall, defined as:

$$u_* \equiv \sqrt{\frac{\tau_w}{\rho}}$$

In this linear sublayer region in turbulent boundary layers, Reynolds Stresses are negligible and the shear stress is linear, allowing for accurate measurements of the wall stress. In order to determine the height of this layer in our experiment, we can use

computational results for the friction coefficient and calculate an expected $y$ at $y^+ = 5$, which is the upper-bound in which this linear assumption may apply. Combining the equations for the friction coefficient and the non-dimensional wall distance, we achieve the following expression:

$$y^+ = \frac{y}{\nu}\sqrt{\frac{C_f {U_\infty}^2}{2}}$$

Setting our $y^+ = 5$ and rearranging for $y$, this expression becomes:

$$y = 5\nu\sqrt{\frac{2}{C_f {U_\infty}^2}}$$

So as not to apply circular reasoning to our problem, it is necessary to select expected values of $C_f$ from experimental and/or computational results from other sources. Lynntech computed a theoretical model for $C_f$ vs. x/c using a the Vortex Panel method to solve for the inviscid flow, the Thwaites-Walze method applied to laminar regimes, and the Moses integral method applied for the turbulent portions of the wing after a predicted transition to turbulent flow at 0.25c [13]. This curve is shown in Figure 30. The curve provided by Lynntech closely follows both qualitative and quantitative behavior examined in several computation and experimental studies involving the wings with a NACA 0012 airfoil shape [15][16]. Discrepancies between predicted and experimental values of friction coefficient will be examined after expected viscous sublayer heights are calculated.

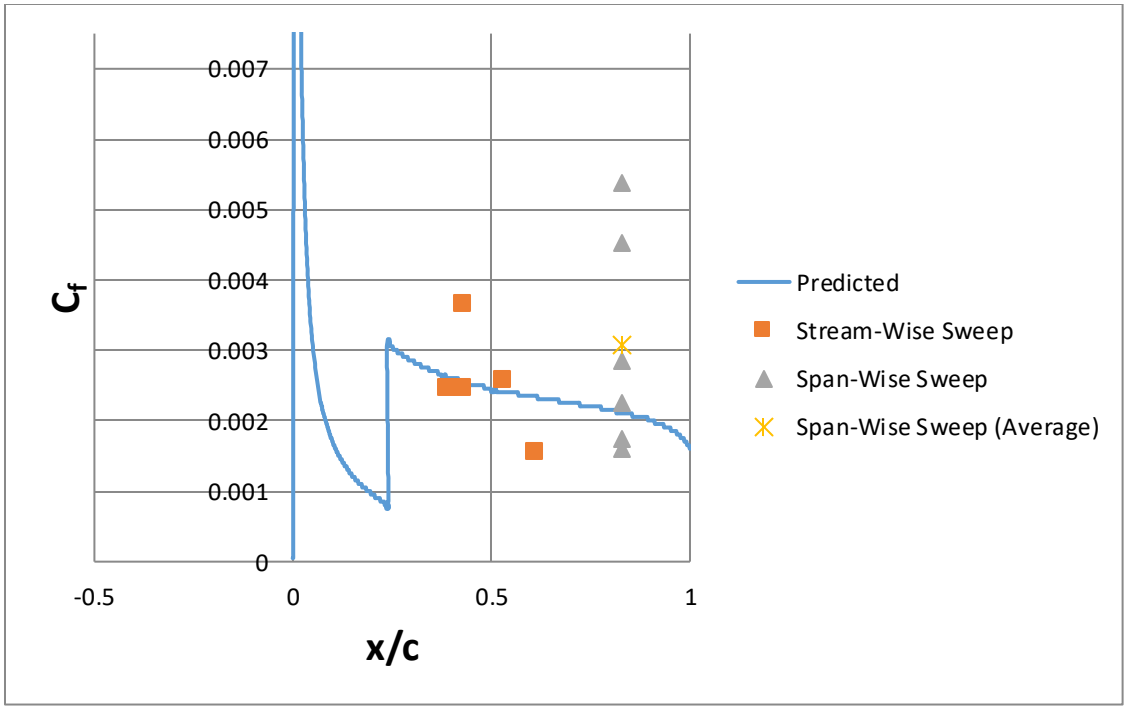


*Figure 30 - Experimental vs. Predicted Friction Coefficient (Credit: Lynntech for Predicted Curve)*

Using the equation described above along with the values extracted from this curve using Data Thief III, it is possible to calculate an approximate viscous sublayer height at various stream-wise locations along the wing. Figure 31 shows this approximate value for the viscous sublayer height at various locations along the wing. These heights vary from about 52-58 µm depending on location. Clearly, if the center of the hot film is about 55 µm above the surface of the wing at its lowest location (the measurement used to calculate the wall stress), this means that our average velocity reading is just at the edge of the linear sublayer. This should yield a wall stress measurement that is at least close to the actual local value at the wall. For a more accurate reading, a Reynolds Stress model such as the one proposed by Durbin [17]

could be used, but for this data set the sensing area is too large for a precisely-quantified value of $y^+$ and any model would involve an average over a large area in which Reynolds Stress changes rapidly, diminishing the model's usefulness in making the measurement more accurate. Still, these readings most-likely took place within the viscous sublayer ($y^+ <$ ~30), so if Reynolds Stress could be subtracted from the overall value, it would be possible to have greater confidence in the calculated wall stress at that location.

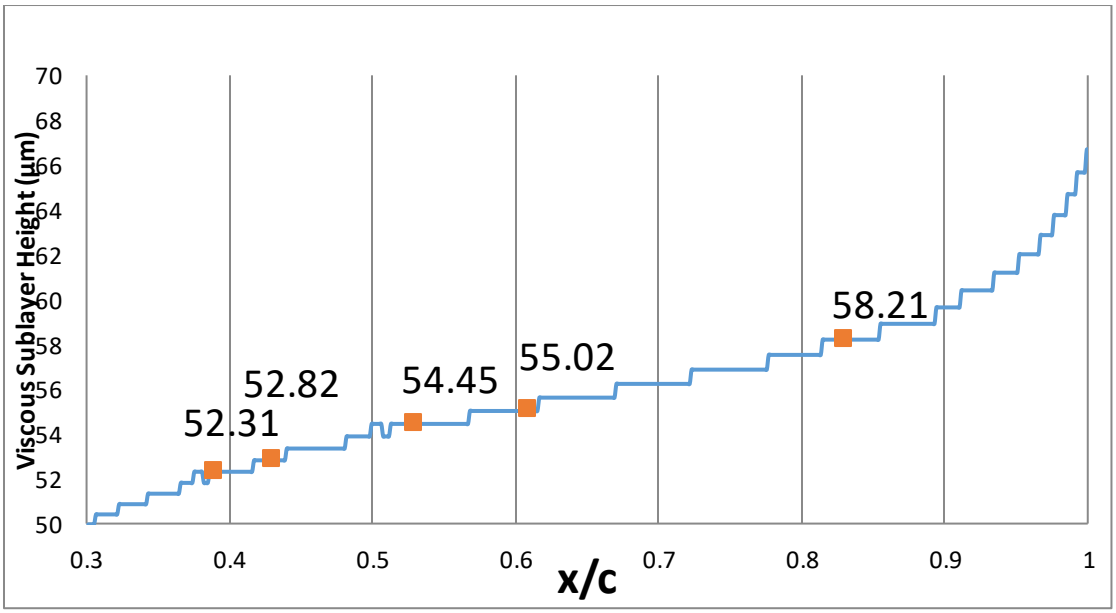


*Figure 31 - Viscous Sublayer Height Based on Lynntech Friction Coefficient Calculations*

Comparisons of individual measurements of the nominal boundary layer to predicted values can be useful in determining which points are the most trustworthy in the sample as well as predicting overall random error. In the stream-wise sweeps, calculated values for nominal friction coefficient were all within 7% of the predicted values with the exception of two points, as shown below in Table 3.

*Table 3 - Discrepancy Between Experimental and Predicted Friction Coefficient for Stream-Wise Sweep*

| x/c | $C_f$ | % Discrepancy |
|---|---|---|
| 0.39 | 0.002466 | -5.42 |
| 0.43 | 0.00245 | -4.19 |
| 0.43 | 0.00364 | 42.35 |
| 0.53 | 0.002571 | 6.83 |
| 0.61 | 0.001546 | -34.40 |
| **Average** | | 18.64 |

It is interesting to note that the second sweep of the nominal boundary layer at 0.49c is the point with the highest error from the predicted value. Considering the strong agreement between the profiles with the plasma actuators on, it may be wise to throw out this data point, which would suggest that the previously discussed possibility of a periodic behavior for drag behind the actuators is more likely to be correct. Additionally, the drag increase seen at the 0.61c location could be complete wiped out by the predicted value of $C_f$, which assuming an accurate measurement for the actuators on reading would result in a drag *decrease* of 27%.

Results for the span-wise sweep are a bit more startling. Shown in Table 4, they show a much greater discrepancy in the nominal values for $C_f$ than the stream-wise sweep. The reason for this difference in both precision and accuracy is unclear. Although the average discrepancy in the stream-wise set was 18.64%, this error was much smaller with the two egregious outliers excepted. On the other hand, the discrepancy of the average value for the 0.83c stream-wise location during the span-wise sweep was a full 45.5% higher than the predicted value. This is especially strange considering that the

same sets of procedures were used to produce these results, with the added advantage of a depth gauge giving extremely accurate measurements between data points.

*Table 4 - Discrepancy Between Experimental and Predicted Friction Coefficient for Span-Wise Sweep*

| z/c | $C_f$ | % Discrepancy |
|---|---|---|
| 0.043 | 0.001596 | -24.21 |
| 0.064 | 0.004532 | 115.21 |
| 0.106 | 0.00286 | 35.81 |
| 0.149 | 0.005384 | 155.67 |
| 0.149 | 0.001747 | -17.04 |
| 0.170 | 0.002265 | 7.56 |
| **Average** | 0.003064 | 45.50 |

In any case, it may be useful to compare our calculated friction coefficient values with plasma actuators on with the predicted nominal value. This is shown in Table 5. It is noteworthy that a comparison to the predicted value of $C_f$ yields a local drag increase at the 0.106c and the 0.149c locations which previously showed a reduction in drag.

In general, however, the procedure used to perform the sweeps had a pivot point (transition from actuators off to actuators on) at the lowest measured wall-normal location. This means that, in general, a location with a nominal friction coefficient that is close to the predicted value should be considered to be more trustworthy than a location whose nominal friction coefficient is far from the predicted value. Several points whose calculated $C_f$ are very close to the predicted value show drag reduction, namely, the 0.39c and 0.53c locations in the stream-wise sweep and the 0.043c starboard and 0.17c starboard locations at 0.83c in the span-wise sweep. Other locations which showed drag

reduction may in fact still have lower wall stresses and friction coefficients, but this is harder to ascertain from the available data.

*Table 5 - Comparison of Drag Reduction from Measured vs. Predicted Nominal Boundary Layer*

| | Spanwise Location (Right of Actuator 5) | | | | | | |
|---|---|---|---|---|---|---|---|
| | **0.043c** | **0.064c** | **0.106c** | **0.149c(1)** | **0.149c(2)** | **0.170c** | **Predicted Value** |
| **Actuators Off** | | | | | | | |
| $\tau_w$ (Pa) | 1.5389 | 4.3691 | 2.7571 | 5.1905 | 1.6836 | 2.1839 | 2.0300 |
| $C_f$ | 0.001596 | 0.004532 | 0.00286 | 0.005384 | 0.001747 | 0.002265 | 0.002106 |
| **Actuators On** | | | | | | | |
| $\tau_w$ (Pa) | 0.853248 | 1.453546 | 2.472655 | 4.335456 | 3.474546 | 1.965817 | |
| $C_f$ | 0.000885 | 0.001508 | 0.002565 | 0.004497 | 0.003604 | 0.002039 | |
| **% Reduction** | 44.55405 | 66.73133 | 10.3177 | 16.47379 | -106.37 | 9.985457 | |
| **vs. Predicted** | **57.96887** | **28.39811** | **-21.8033** | **-113.565** | **-71.1566** | **3.163572** | |

Other sources of random error exist within the data set. The decision of whether or not to keep lowering the probe into the boundary layer was partially made via visual inspection. If any space could be seen between the probe tip and the wing (through clear plexiglass at a distance of approximately 2 ft.), the probe would be lowered. If no space could be seen and if the measured velocity was lower than ~20% of the freestream value, the probe would be stopped and the plasma actuators turned either on or off. The human eye at 20/20 vision has the ability to resolve a spatial pattern separated by one minute of arc [18]. At a distance of 2 ft (0.6091 m), this means that the maximum distance possible from the bottom of the hot film prongs to the surface is 177.3 μm. At first glance, this appears to be a large distance compared to the very small linear sublayer (about 1/3 of

this distance), but often decisions to stop descending were made instead on the basis of measured velocity values. With the traversing axis' movement resolution of 75 μm, however, care was needed to ensure that the hot film was not damaged by contact with the surface. This random error could very well describe the bulk of points which showed nominal friction coefficient behavior far from the predicted values.

One other potential source of random or systematic error is electromagnetic interference (EMI) when the plasma actuators are engaged, which could induce a change in voltage in the hot film velocity measurements. In order to test this, several measurements were taken both with and without plasma actuators engaged. Figure 32 shows the results of these samples. The electromagnetic signal is negligible, particularly at lower velocities. This means that the velocity measurements low in the boundary layer shouldn't be changed significantly by EMI from the plasma actuators.

An additional potential source of error is tunnel heating. If the tunnel changed temperature over the course of testing, this would result in differences in the velocity readings because the calibration is only valid for the room-temperature conditions. Because internal wind tunnel measurements were not taken before and after each sweep, this might seem like a legitimate concern. This is mitigated by the fact that boundary layer profiles with and without the plasma actuators pulsing were taken in quick succession. Because these measurements are compared to each other rather than to other points on the wing, this makes comparisons between the two valid even if the tunnel temperature changed slightly over a few hours of testing several different locations.

In addition to tunnel heating, near-wall measurements could be affected from radiative heat transfer between the hot film and the relatively cool surface of the wing. Additionally, if there was contact between the prongs and wing surface, conductive heat transfer could further skew results.

In light of all of these potential sources of error, an additional analytical method was suggested to compare results to points within the boundary layer that would be more easily measured. The log-layer, which behaves very predictably over a much larger physical distance than the linear sublayer, could be examined and correlated with skin friction using known experimental values. These values could be used to validate near-wall measurements and will be discussed in the proceeding section, including their own potential error.

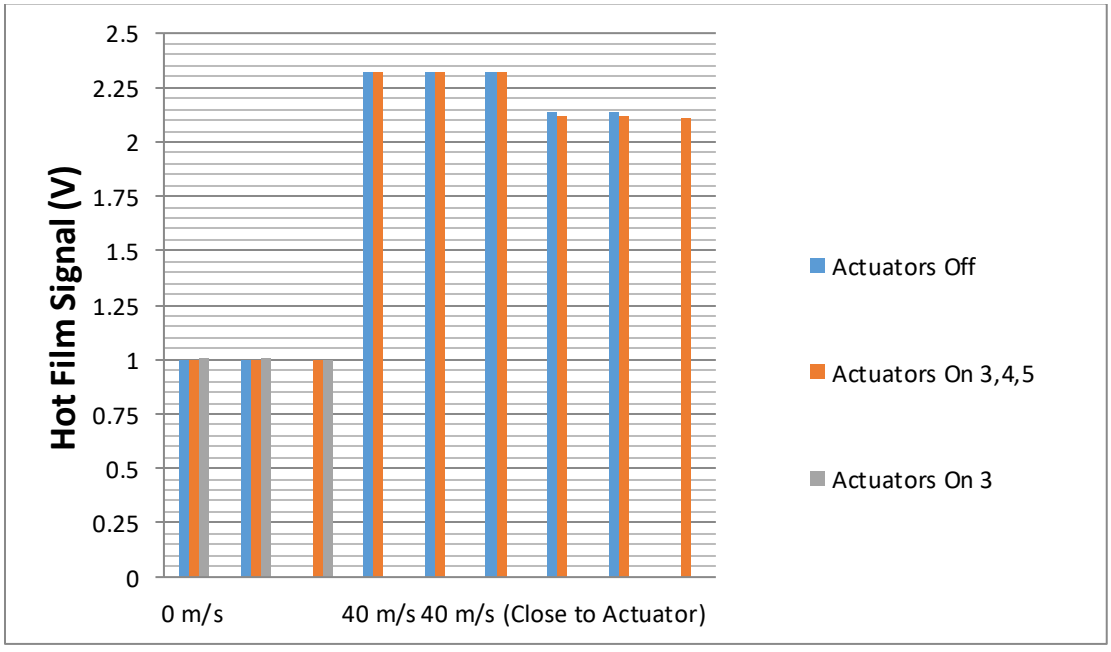


*Figure 32 - Hot Film Electromagnetic Interference*

*Log-Layer Analysis and Validation*

As distance away from the surface increases, relations described for the viscous sublayer become invalid. Instead, as laid out in the approach from White [3] below, the flow behaves logarithmically in terms of so-called "inner variables." One of these inner variables, $y^+$, has already been defined. The other variable, the dimensionless velocity $u^+$, is simply the average velocity divided by the friction velocity so that:

$$u^+ \equiv \frac{\bar{u}}{u_*}$$

This layer's logarithmic behavior may be described by the following equation, known as the "law of the wall:"

$$u^+ = \frac{1}{\kappa} \ln y^+ + B$$

From experiments, the parameters $\kappa$ and $B$ have been determined to be constants with values of 0.41 and 5.0, respectively. This behavior has been shown to be valid for values of $y^+$ between about 35 and 350.

Taking this result and expanding the relations for $u^+$, $y^+$, and $u_*$ based on their definitions, this equation may be rewritten as:

$$\frac{\bar{u}}{\sqrt{\frac{\tau_w}{\rho}}} = \frac{1}{0.41} \ln \frac{y\sqrt{\frac{\tau_w}{\rho}}}{\nu} + 5.0$$

In turn, this equation may be rearranged and rewritten in terms of $C_f$ as:

$$C_f = \frac{2}{{U_\infty}^2}\left[\frac{\bar{u}}{\frac{1}{0.41}\ln\frac{y}{\nu}\sqrt{\frac{C_f {U_\infty}^2}{2}} + 5.0}\right]^2$$

Since this equation is valid for all locations in the log-layer, each velocity measurement in that region should follow the relation. By using an initial guess from previously-calculated results for $C_f$ on the right-hand side and iterating to convergence, a value of $C_f$ that satisfies this equation may be calculated for each measurement within the log-layer. Since each wing location surveyed has several locations believed to be in this region, this should result in more data points which could corroborate the previous results taken from the near-wall measurements.

Unfortunately, calculated values of $C_f$ were not consistent throughout the log-layer. Instead, predicted $C_f$ was lowest and closest to the measured and numerically-predicted values at lower values of $y^+$. Results may be seen in Figure 33 below.

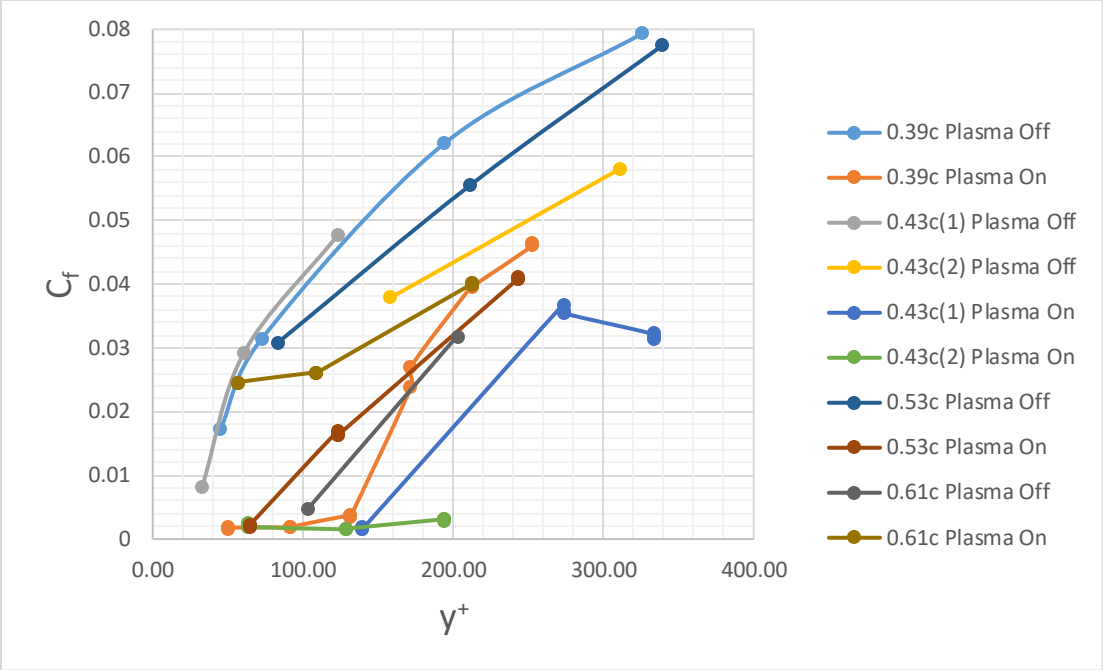


*Figure 33 - Log-Layer Analysis - $y^+$ vs. $C_f$*

It may be observed from the figure that predicted $C_f$ is consistently smaller lower in the boundary layer (with the exception of one point in the 0.43c position). Additionally, values of $C_f$ are consistently smaller across the board for the plasma-on boundary layers, with the exception of the 0.61c position. This is mostly consistent with previous results, with the exception that in the log-layer, calculated $C_f$ values are lower for both sets of measurements at 0.43c with the plasma actuators on.

At the time of writing, it is not understood why calculated values of $C_f$ fluctuate through the log layer. This could be due to any number of factors discussed in the sources of error above, and the measurement should be repeated in future experiments in order to validate these results. That being said, it appears that even higher in the

boundary layer, calculated values of $C_f$ are reduced when the plasma actuators are pulsed. This can only help to strengthen the previous results of the experiment.

**Overall Wing Drag Measurements**

Measurements comparing overall drag with and without plasma actuator activity show some signs of potential overall drag reduction. While it cannot be overstated that these small numbers of plasma actuators pulsed at one time were not expected to have a significant impact on overall drag measurements, several conditions tested showed some potential for reduction in overall drag. The precision of the pyramidal balance and electromagnetic interference are a potential issue for these tests, but these considerations will be discussed in the error analysis sub-subsection.

Figure 34, Figure 35, and Figure 36 show drag force measurements taken from the pyramidal balance for different combinations of actuators. Results vary from test to test, but in general both the low- and high-frequency pulsed actuators show reductions from the nominal drag, although these reductions in drag are small (maximum 2%), this is expected due to the relatively small number of plasma actuators on the wing and the lack of proper tuning of the actuators to the wing to produce maximum drag reduction.

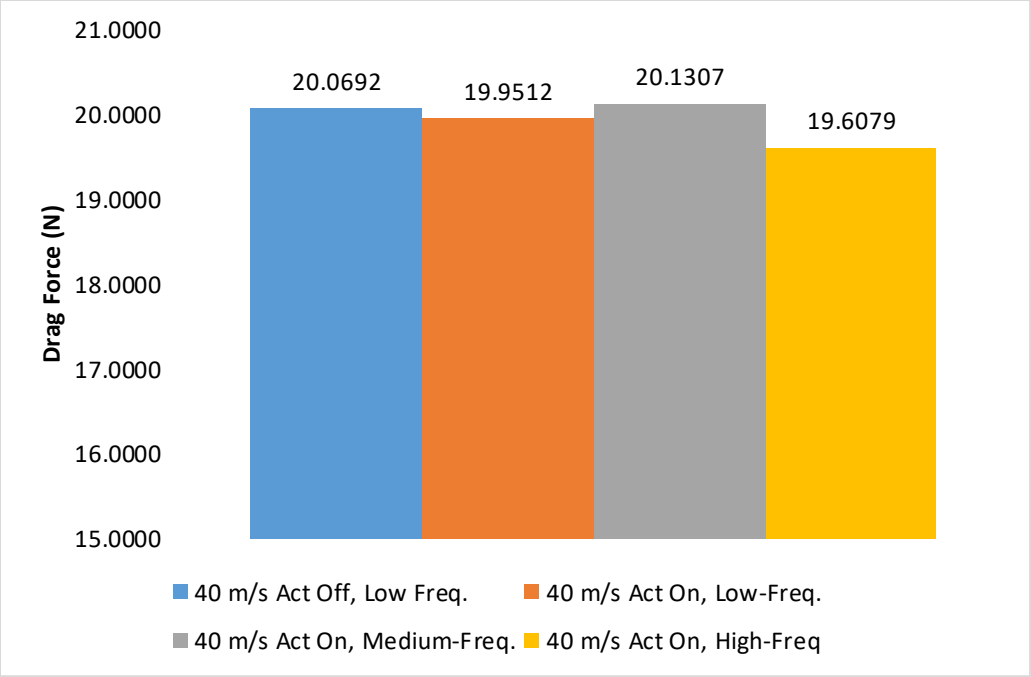


*Figure 34 - Total Wing Drag - Actuators 3-5*

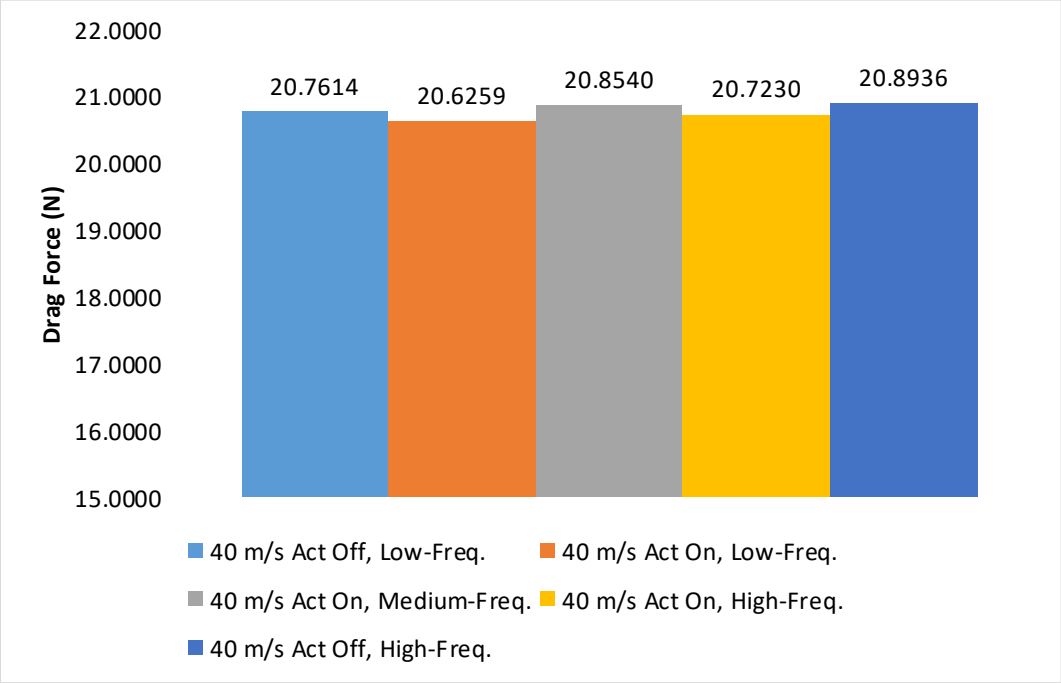


*Figure 35 - Total Wing Drag - Actuators 1-6*

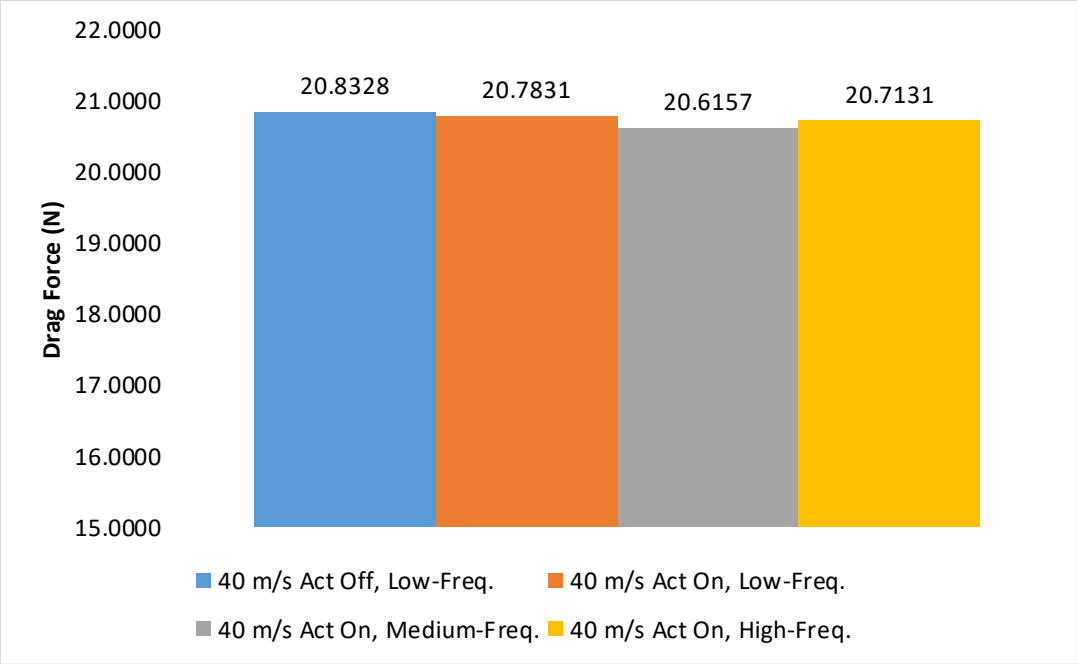


*Figure 36 - Total Wing Drag - Actuators 2-7*

Results summarized in Table 6 below show several interesting trends. Namely, overall drag is reduced by the activation of the plasma actuators in all cases except the first two cases for the medium-frequency pulses. That this reduction in overall drag is both significant and measurable with as few as three plasma actuators spaced over the surface of the wing is a very promising development which seems to agree with the results seen in the boundary layer measurements.

*Table 6 - Summary of Overall Wing Drag Results*

| Condition | Actuator Numbers | Avg Voltage | Drag Force (N) | % Reduction |
|---|---|---|---|---|
| 40 m/s Act Off, Low-Frequency | 3,4,5 | 4.6629 | 20.0692 | |
| | 1,2,3,4,5,6 | 4.6498 | 20.7614 | |
| | 2,3,4,5,6,7 | 4.6485 | 20.8328 | |
| 40 m/s Act On, Low-Frequency | 3,4,5 | 4.6651 | 19.9512 | **0.59%** |
| | 1,2,3,4,5,6 | 4.6524 | 20.6259 | **0.65%** |
| | 2,3,4,5,6,7 | 4.6494 | 20.7831 | **0.24%** |
| 40 m/s Act On, Medium-Frequency | 3,4,5 | 4.6618 | 20.1307 | **-0.31%** |
| | 1,2,3,4,5,6 | 4.6481 | 20.8540 | **-0.45%** |
| | 2,3,4,5,6,7 | 4.6526 | 20.6157 | **1.04%** |
| 40 m/s Act Off, High-Frequency | 1,2,3,4,5,6 | 4.6473 | 20.8936 | |
| 40 m/s Act On, High-Frequency | 3,4,5 | 4.6716 | 19.6079 | **2.30%** |
| | 1,2,3,4,5,6 | 4.6506 | 20.7230 | **0.82%** |
| | 2,3,4,5,6,7 | 4.6507 | 20.7131 | **0.57%** |

*Error Analysis*

There are three main sources of potential error in the overall drag tests – variance in the response of the pyramidal balance (related to the balance's precision), EMI, and inconsistencies in drag due to the model contacting the side walls.

The pyramidal balance attached to the model sting was manufactured by the Aerolab, LLC in the 1980s. Attempts to find documentation on the precision of this instrument were unsuccessful, as Aerolab no longer keeps records on systems that old. However, from the calibration curve an estimate of the variance $\sigma^2$ in the voltage measurements may be calculated using the Mean Square Error, which is expressed as:

$$MSE = \frac{\sum_{i=1}^{n}(y_i - \hat{y}_i)^2}{n-2}$$

where $y_i$ is the exact value of the voltage for a given applied load, $\hat{y}_i$ is the expected voltage for a given load (from the linear regression), and $n$ is the population size. Because we are using a sample of the population to determine both the slope and intercept of the regression line, we must divide by the population size minus two due to a loss of two degrees of freedom [18]. Based on the calibration curve for the pyramidal balance, the MSE and therefore a good estimate for $\sigma^2$ is $2.21 \times 10^{-4}$ V. This means that the standard deviation of the sample is approximately $1.49 \times 10^{-2}$ V, which is equivalent to a difference in load of 0.833 N, or approximately 4.01% of the total load at 40 m/s with no actuators applied. Although this is a very conservative approach given the linearity of our signal ($R^2 = 0.9975$), this means that all observed drag measurements are within the margin of error of the system as it is currently known. Back-calibration using more points could bring this error down to manageable levels.

The second possible source of error was EMI, which was investigated in much the same was as for the boundary layer measurements. With the wind tunnel turned off, voltage signals from the balance (nominally zero since the drag should be zero with no air flow) were taken and plotted, with differences in voltages converted to a drag force. Since the fit is linear, any increase or decrease in measured load due to EMI should translate to drag force at any freestream velocity. Table 7 shows these results, which are significant. For the actuators pulsing at 1 Hz, measured drag loads are increased by 0.02-0.024 N, which translate to an overshoot of drag reduction by up to 0.12%. On the other hand, load measurements taken with the plasma actuators pulsing at 10 Hz and 50 Hz will underestimate the drag load by 0.22% and 0.37%, respectively.

*Table 7 - Wing Drag EMI Test Results*

| Condition | Actuator Numbers | Avg Voltage | Drag Force (N) | Change in Drag Force (N) |
|---|---|---|---|---|
| 0 m/s, Act Off | 3,4,5 | 5.0430 | -0.0449 | |
| 0 m/s, Act On, Low-Frequency | 3,4,5 | 5.0425 | -0.0206 | **0.0243** |
| | 2,3,4,5,6,6 | 5.0426 | -0.0241 | **0.0208** |
| 0 m/s, Act On, Medium-Frequency | 2,3,4,5,6,7 | 5.0438 | -0.0889 | **-0.0440** |
| 0 m/s, Act On, High-Frequency | 2,3,4,5,6,8 | 5.0444 | -0.1216 | **-0.0767** |

The third source of error is random and very hard to quantify, and involves the difference in loading at during the tests of actuators 3, 4, and 5. These tests consistently yielded lower overall drag loads than the tests with up to 6 actuators engaged. This could be due to incidental contact of the model with the side-walls, which would reduce the drag load since friction force would resist movement.

With all three of these sources of error considered, all of the reductions in drag are within the error bounds of the system. Although this is the case, it is the opinion of the author that all low- and high-frequency cases showing a reduction in drag after the EMI adjustment without exception at least demonstrates a significant possibility that some overall drag reduction was achieved. A careful recalibration of the pyramidal balance could very well reduce the variance in the load data significantly, and this is recommended in the future.

## CONCLUSIONS AND RECOMMENDATIONS

Boundary-layer measurements showed convincing evidence of a local reduction in skin-friction drag. The near-wall low-velocity region in the area of influence of the actuators is consistent with the computational findings by Du and Karniadakis, and is evidence (albeit inconclusive) of disruption of the near-wall low-velocity streaks believed to be chiefly responsible for turbulence production in the boundary layer. Such reductions were observed up to 0.32c downstream of the plasma actuators and 0.17c starboard of one plasma actuator, which would suggest a relatively small number of actuators necessary to reduce drag over the entire surface of the wing. As previously stated, however, it must be noted that without extensive flow field analysis behind the plasma actuators (not just point measurements), the mechanism for any observed drag reduction may only be hypothesized based on available qualitative flow behavior.

Potential sources for error in this case seem to be outweighed by the consistency with which these results were produced. Random errors in wall-distance cannot explain the consistent reduction in wall shear stress at nearly every location and every sampling point. Coupled with the extremely low error in the velocity measurements because of the precision of the hot film used, this suggests that reductions in local drag were achieved. Preliminary analysis of the log-layer shows reductions in friction coefficient, but an anomaly in the behavior of the friction coefficient throughout the log-layer renders these results hopeful, but inconclusive.

Overall drag measurements are less conclusive in some respects. Variance in the calibration curve, a linear regression through ten points, suggests that the system is not

extremely precise in measuring loads. This makes the small observed decreases in drag somewhat suspect, although this variance does not account for all observed drag reduction. Electromagnetic interference also produced artificially-low drag readings in medium- and high-frequency cases, although these do not in all cases account for the total reduction in drag observed. In particular, the low-frequency case showed consistent reduction in overall drag despite the EMI effect artificially *increasing* the recorded drag measurements by a slight amount. This further suggests that observations in the boundary layer measurements are consistent with reduction in turbulent drag rather than some other phenomenon such as flow separation.

Thus, it is recommended that this effect is studied further with a more robust experimental design and more precise instrumentation and measurement systems. The use of a TSI Model 1218 Standard Boundary Layer Probe with a T1.5 Tungsten hot wire (with a sensing area of 3.8μm) would be able to provide more precise measurements in the boundary layer region. The fast frequency response and small size of this probe would also allow for Reynolds-Stress modeling of values at the edge of the laminar sublayer, allowing for more reliable measurements. Additionally, the increased frequency response could be used to perform spectral analysis to confirm the presence of a span-wise traveling wave. Turbulence statistics could be used in the lower portion of the boundary layer to determine if the probe was able to reach the laminar sublayer in which reliable wall shear stress measurements may be made. A model designed for a thicker viscous sublayer could be helpful in this endeavor, as long as the global Reynolds number was still high enough to be comparable to this test's results. A more

precise 3D traversing system complete with stepper motors and an absolute encoder would be able to ensure, along with precise measurements of the model and test section configuration, that the probe could be brought safely into this region. This is an extremely challenging measurement for any technique, however, and considerable cost could be incurred only to find additional sources of error present.

Flow visualization techniques such as PIV could be used to attempt to capture the span-wise traveling wave (or determine if such a phenomenon is not present). Flow following of the particles and reflections would be difficult, but in the right wind tunnel this measurement could be possible. Finally, the plasma actuators should be tuned to reliably produce a wave that is tuned to the system. Phasing the actuators and varying the frequency and intensity would all help determine the configuration where maximum drag reduction is possible. All of these measures are cost- and time-prohibitive, but results in this experiment show enough promise to warrant further investigation.

## REFERENCES


[1] Anderson, John D. *Hypersonic and High-temperature Gas Dynamics*. Reston, VA: *American Institute of Aeronautics and Astronautics*, 2006. Print.

[2] Anderson, John D., Jr. *Fundamentals of Aerodynamics*. 5th ed. New York: *McGraw-Hill*, 2011. Print.

[3] White, Frank M. *Viscous Fluid Flow*. 3rd ed. New York: *McGraw-Hill Higher Education*, 2006. Print.

[4] Schlichting, Hermann. *Boundary-layer Theory*. New York: *McGraw-Hill*, 1979. Print.

[5] "Wright 1901 Wind Tunnel." *Wright 1901 Wind Tunnel*. NASA Glenn Research Center, 12 June 2014. Web.

[6] Kline, S. J., W. C. Reynolds, F. A. Schraub, and P. W. Runstadler. "The Structure of Turbulent Boundary Layers." *Journal of Fluid Mechanics*, Vol. 30.04, 1967: 741-73. *Cambridge Journals*. Web.

[7] Head, M. R., and P. Bandyopadhyay. "New Aspects of Turbulent Boundary-layer Structure." *Journal of Fluid Mechanics,* Vol. 107, 1981, pp. 297-338. *Cambridge Journals*. Web.

[8] Bechert, D. W., and M. Bartenwerfer. "The Viscous Flow on Surfaces with Longitudinal Ribs." *Journal of Fluid Mechanics,* Vol. 206, 1989, pp. 105-29. *Cambridge Journals*. Web.

[9] Du, Y and Karniadakis, G., "Suppressing Wall Turbulence by Means of a Transverse Traveling Wave," *Science*, Vol. 288, May 2000.

[10] Rediniotis, Othon, Dimitris Lagoudas, Raghavendran Mani, Lance Traub, Richaed Allen, and George Karniadakis. "*Computational and Experimental Studies of an Active Skin for Turbulent Drag Reduction*." 1st AIAA Flow Control Conference. St. Louis, Missouri. *AIAA Aerospace Research Central*. 26 June 2002. Web.

[11] Wilkinson, Stephen P., "*Investigation of an oscillating surface plasma for turbulent drag reduction*," *AIAA 41st Aerospace Sciences Meeting and Exhibit*, AIAA 2003-1023, January 2003.

[12] Jukes, Timothy M., Kwing-So Choi, Graham A. Johnson, and Simon J. Scott. "*Turbulent Drag Reduction by Surface Plasma through Spanwise Flow Oscillation*." *AIAA Aerospace Research Central*. Proc. of 3rd AIAA Flow Control Conference, San Francisco, CA. N.P., 8 June 2006. Web.

[13] Lynntech, Inc., *Drag Reduction through Pulsed Plasma Actuators: Phase I Final Report*, Proprietary Internal Technical Report, December 2015.

[14] B. Tummers, DataThief III. 2006. Web.

[15] Nowak, Lisa M. *Computational Investigations of a NACA 0012 Airfoil in Low Reynolds Number Flows*. Thesis. Naval Postgraduate School, 1992. Fort Belvoir, VA: Defense Technical Information Center, 1992. *DTIC*. Web.

[16] Becker, John V. *Boundary-Layer Transition on the N.A.C.A. 0012 and 23012 Airfoils in the 8-Foot High-Speed Wind Tunnel*. Rep. no. 65682. Langley Field, VA: NACA, 1940. *DTIC*. Web.

[17] Durbin, P. A. "A Reynolds Stress Model for Near-wall Turbulence." *Journal of Fluid Mechanics,* Vol. 249, 1993, pp. 465-98. *Cambridge Journals*. Web.

[18] Simon, Laura J. "Lesson #1: Simple Linear Regression." *Lesson #1: Simple Linear Regression*. The Pennsylvania State University, 2004. Web.